Bodine Journal

Volume 2 | Issue 1 Article 6

2009

Download Entire Bodine Journal Volume 2, Issue 1, 2009

Jefferson
Kimmel Cancer Center
NCI-designated

Vol 2, Issue 1 | Fall 2009

BODINE JOURNAL

Inside

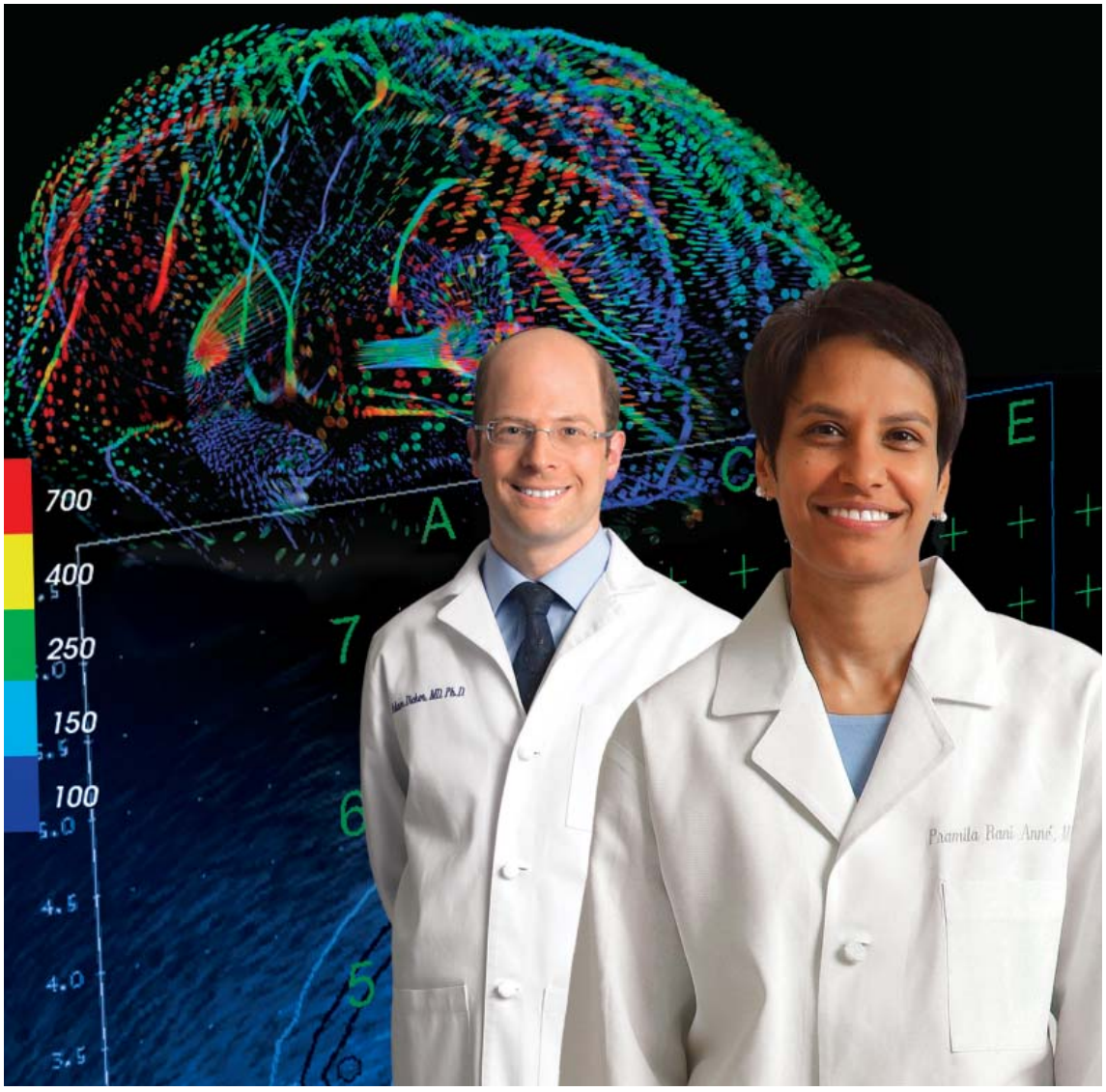

A publication of Thomas Jefferson University, Department of Radiation Oncology

NCI·CC
A Cancer Center Designated by the National Cancer Institute

THOMAS JEFFERSON UNIVERSITY AND HOSPITALS

BODINE JOURNAL

Vol 2, Issue 1 | Fall 2009

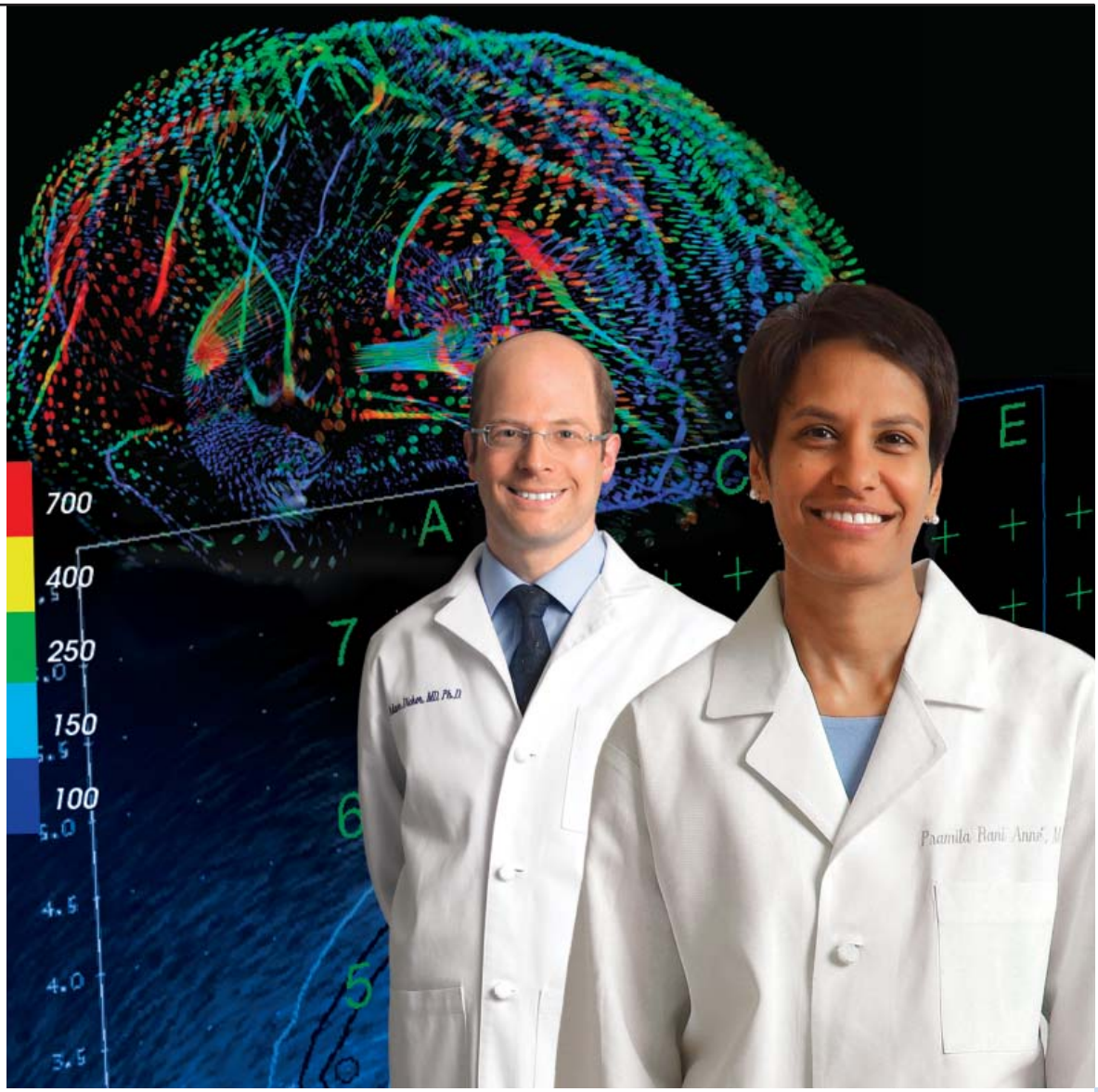

A publication of Thomas Jefferson University, Department of Radiation Oncology

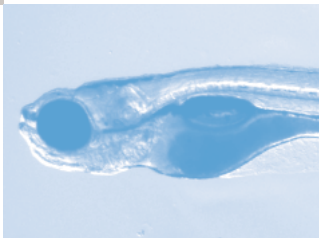

General Information

Correspondence, inquiries, or comments may be submitted to the Editor, *Bodine Journal*, Jefferson Kimmel Cancer Center- Bodine, 111 S. 11th St., Philadelphia, PA 19107 or email at: BODINEjournal@jeffersonhospital.org

www.kimmelcancercenter.org/kcc/radonc/bodine_journal/2009FallBodineJournal.pdf

ISSN 2152-2030

Table of Contents

Articles

Departmental Information

Names in Bold: Members of the Department of Radiation Oncology, Thomas Jefferson University

Nuclear Factor κB Inhibitors Alleviate and the Proteasome Inhibitor PS-341 Exacerbates Radiation Toxicity in Zebrafish Embryos

Borbala Daroczi,[1] Gabor Kari,[1] Qing Ren,[1] Adam P. Dicker,[1,3] and Ulrich Rodeck[2,3]

[1]Departments of Radiation Oncology, and [2]Dermatology and Cutaneous Biology, and [3]Kimmel Cancer Center, Thomas Jefferson University, Philadelphia, Pennsylvania

Reprinted with permission from the American Association of Cancer Research, "Nuclear factor κB inhibitors alleviate and the proteasome inhibitor PS-341 exacerbates radiation toxicity in zebrafish embryos", Moleculaer Cancer Therapy, 2009;8(9), pages 2625-2634.

Abstract

Inflammatory changes are a major component of the normal tissue response to ionizing radiation, and increased nuclear factor κB (NF-κB) activity is an important mediator of inflammatory responses. Here, we used zebrafish embryos to assess the capacity of two different classes of pharmacologic agents known to target NF-κB to modify radiation toxicity in the vertebrate organism. These were proteasome inhibitors, including lactacystin, MG132, and PS-341 (Bortezomib/VELCADE), and direct inhibitors of NF-κB activity, including ethyl pyruvate (EP) and the synthetic triterpenoid CDDO-TFEA (RTA401), among others. The proteasome inhibitors either did not significantly affect radiation sensitivity of zebrafish embryos (MG132, lactacystin) or rendered zebrafish embryos more sensitive to the lethal effects of ionizing radiation (PS-341). Radiosensitization by PS-341 was reduced in fish with impaired p53 expression or function but not associated with enhanced expression of select p53 target genes. In contrast, the direct NF-κB inhibitors EP and CDDO-TFEA significantly improved overall survival of lethally irradiated zebrafish embryos. In addition, direct NF-κB inhibition reduced radiation-induced apoptosis in the central nervous system, abrogated aberrations in body axis development, restored metabolization and secretion of a reporter lipid through the gastrointestinal system, and improved renal clearance compromised by radiation. In contrast to amifostine, EP and CDDO-TFEA not only protected against but also mitigated radiation toxicity when given 1 to 2 hours postexposure. Finally, four additional IκB kinase inhibitors with distinct mechanisms of action similarly improved overall survival of lethally irradiated zebrafish embryos. In conclusion, inhibitors of canonical pathways to NF-κB activation may be useful in alleviating radiation toxicity in patients. [*Mol Cancer Ther* 2009;8(9):2625-34]

Introduction

Normal tissue damage limits the dose of ionizing radiation that can be safely administered to treat neoplastic disease. A well-known example of this problem is inflammation of the oral mucosa and of the lining of the gastrointestinal tract in tumor patients receiving chemotherapy or radiation.[1] Depending on the area of the body treated with radiation, other organ sites including the lungs and the pericardium also manifest radiation-induced inflammation. A pervasive feature of ionizing radiation–associated inflammation is the increased presence of proinflammatory cytokines including tumor necrosis factor-α (TNF-α) and interleukin-6, both locally and in the circulation.[2] In contrast to intracellular regulators of the DNA damage response, these and other inflammatory mediators act in a paracrine fashion affecting diverse cell types in the tissue microenvironment or even at a distance.[3] This circumstance highlights the necessity to use animal models to investigate the relative contribution of inflammatory changes to the overall response to radiation-induced cell and tissue injury in a multicellular organism. In recognition of this need, we recently established zebrafish embryos as a facile vertebrate *in vivo* system to monitor the effects of radiation protectors on normal tissues during development.[4]

The nuclear factor κB (NF-κB) family of transcription factors represents a diverse and shared signaling mechanism activated during cell stress responses.[5] In addition, deregulated NF-κB signaling has been implicated in the malignant phenotype and treatment resistance of select tumor forms.[6-10] The canonical pathway to NF-κB activation leads to IκB kinase β (IKKβ)-dependent phosphorylation and subsequent proteasomal degradation of the NF-κB inhibitor IκB, increased nuclear presence of NF-κB dimers, and enhanced NF-κB–dependent transcriptional activity.[5]

Whole-body radioprotection through anti-inflammatory agents has very recently been shown in animal models. Specifically, certain triterpenoids (CDDO and derivatives thereof) have been shown to selectively protect normal mouse tissues against the deleterious effects of ionizing radiation.[11] Furthermore, ethyl pyruvate (EP), a derivative of the end product of glycolysis, similarly protects normal cells against the deleterious effects of radiation both *in vitro* and in mice.[12] Among other molecular targets, both drugs inhibit activation of NF-κB. EP inhibits NF-κB signaling through direct molecular interaction with a reactive cysteine of the p65 subunit of NF-κB[13] whereas CDDO-TFEA binds to a reactive cysteine (Cys179) of IKKα, thus inhibiting its kinase activity.[14] However, these drugs also target other signaling molecules and pathways of potential relevance to the radiation response, including signal transducers and activators of transcription 3 and Jaks.[15, 16] In addition to these agents proteasome inhibitors have been shown to inhibit NF-κB–dependent transcription, and one of these (PS-341; Bortezomib; VELCADE)

has been Food and Drug Administration–approved for clinical use in patients afflicted with multiple myeloma (for review see refs.[17, 18]). It is presently unknown whether and how proteasome inhibitors affect whole-body radiation sensitivity.

Collectively, these results raised the question whether inhibition of NF-κB activity by different pharmacologic agents contributes to the protection of normal cells and tissues against damage induced by ionizing radiation. Here, we addressed this issue using zebrafish embryos as an *in vivo* model system. We observed that the NF-κB inhibitors EP and CDDO-TFEA afforded protection to zebrafish embryos against the lethal effects of radiation in the pre-exposure and postexposure settings, i.e., when administered hours after radiation exposure. Radiation protection extended to multiple organ sites including the gastrointestinal system and, importantly, was also observed when using additional IKK inhibitors with different modes of action. In contrast, several proteasome inhibitors, including PS-341, did not protect against, but rather moderately exacerbated radiation-associated normal tissue toxicity in zebrafish embryos. These results predict a favorable therapeutic index for the use of inhibitors of canonical pathways to NF-κB activation in combination with radiation therapy.

Materials and Methods

Embryo Harvesting and Maintenance

Zebrafish were mated in embryo collection tanks. Viable embryos were washed and sorted (25 embryos per 60-mm dish) at the one- to two-cell developmental stage, and maintained under normoxic conditions at 28.5°C to enable normal development. Embryo medium was changed at 24, 72, and 120 h postfertilization (hpf). All procedures using live zebrafish were approved by the Institutional Animal Care and Use Committee at Thomas Jefferson University. In select experiments, embryos (24 hpf) were dechorionated by placement in embryo medium supplemented with 50 μg/mL pronase (Sigma) for approximately 10 min at room temperature, then gently agitated with a plastic pipette until the embryos were liberated from the disrupted chorions. After dechorionation, the embryos were rinsed thoroughly with embryo medium, and placed in fresh embryo medium.

Radiation Exposure and Drug Treatments

Pharmacological agents [EP was kindly provided by CDDO-TFEA was from Reata Pharmaceuticals; IKK inhibitor 2 (Weldelolactone), IKK inhibitor 3 (BMS-345541), IKK-2 inhibitor 4, and IKK-2 inhibitor 5 (IMD-0354) were from Calbiochem; MG132 was from Sigma; PS-341 was from Millennium Pharmaceuticals; and lactacystin was from Calbiochem) were dissolved in embryo medium containing <0.1% DMSO. Embryo medium was used as a vehicle control in all experiments. Unless stated otherwise embryos were exposed to ionizing radiation ranging in dose from 0 to 20 Gy at 24 hpf using an X-ray machine (Gulmay Medical) or a ^{137}Cs radiation source. Toxicity analyses for EP (<10 mmol/L), CDDO-TFEA (<10 μmol/L), PS-341 (<10 μmol/L), MG132 (<50 μmol/L), or lactacystin (<10 μmol/L) were conducted by monitoring survival and development of zebrafish embryos for 7 d in the absence of radiation. To determine modulation of radiation-induced toxicity, EP (1 mmol/L) or CDDO-TFEA (1 μmol/L) was added to embryos either 1 h before or up to 3 h after radiation exposure at 24 hpf. The proteasome inhibitors were added to zebrafish embryos 1 h prior to ionizing radiation. After irradiation, zebrafish embryos were maintained at 28.5°C for up to 7 d postfertilization to monitor effects of treatments on survival, morphology, and organ-specific toxicity.

Analysis of Treatment Effects on Zebrafish Survival and Gross Morphology

Dechorionated embryos at 72 hpf were anesthetized with a 1:100 dilution of 4 mg/mL tricaine methanesulfonate (Sigma) and immobilized by placing them on 3% methylcellulose on a glass depression slide. Morphology was assessed visually using a light transmission microscope (Olympus BX51, Olympus) at 40 to 100× magnification, and representative images recorded using a QIMAGING camera and QIMAGING Advanced software (QIMAGING Diagnostic Instruments). Similarly, survival of embryos was assessed visually at 24-h intervals up to 7 days by light microscopy. The criterion for embryonic survival was the presence of cardiac contractions.

Apoptosis Assay

Zebrafish embryos were incubated for 1 h in embryo medium containing modifiers of the radiation response and exposed to 20 Gy at 24 hpf. Six hours after radiation exposure, embryos were stained for 15 min using 5 μg/mL of acridine orange dye (Sigma) and rinsed five times with embryo medium as described previously.[19] Zebrafish embryos were imaged with QIMAGING camera and iVision software; the images were analyzed using ImageJ software.

Detection of ROS

Reactive oxygen species (ROS) levels were measured in dechorionated zebrafish embryos in 96-well plates. Embryos (1 embryo/well) were treated with either vehicle (embryo medium) or EP (1 mmol/L) or CDDO-TFEA (1 μmol/L) in the presence of 5-(and-6)-chloromethyl-2′,7′-dihydrodichlorofluorescein diacetate (CM-H_2DCFA; 500 ng/mL; Molecular Probes) followed by radiation exposure at 24 hpf. The average fluorescence emission at 530 nm following excitation at 490 nm was detected immediately and 2 h after ionizing radiation exposure using a microplate fluorescent reader (BIO-TEK FL 600, BIO-TEK Instruments Inc.). To account for radiation-induced ROS in the embryo medium results were corrected by subtraction of values obtained in wells not containing fish in the presence and absence of pharmacologic agents.

Renal Function Assay

Time-dependent clearance of tetramethylrhodamine-labeled 10-kDa dextran (Molecular Probes) was determined as described previously with minor modifications.[20] Briefly, zebrafish embryos at 24 hpf were exposed to ionizing radiation and maintained in embryo medium. At 72 hpf embryos were anesthetized using a 1:100 dilution of 4 mg/mL tricaine methanesulfonate (Sigma) and dorsally positioned on 3% methylcellulose gel. Tetramethylrhodamine-labeled 10-kDa dextran was injected into the cardiac venous sinus; embryos were kept at 28.5°C, and imaged at 1 and 24 h following microinjection. The average fluorescence emission at 590 nm following excitation at 570 nm was detected at the center of the cardiac area, and the relative intensity was measured using a Leica microscope (Leica Mikroskopie & Systeme GmbH). Images were transformed into grayscale and evaluated with NIH ImageJ software as described.[20]

Morphologic Analysis of the Gastrointestinal System

The functional and morphologic integrity of the developing gastrointestinal system was assessed in zebrafish embryos using PED6, a fluorescent reporter of phospholipase A2 (PLA_2) activity. PED6 is a fluorogenic substrate for PLA_2, which contains a BODIPY FL dye-labeled acyl chain and a dinitrophenyl quencher group.[21] The cleavage of the dye-labeled acyl chain by PLA_2 within cells lining the intestine unquenches the dye and leads to detectable fluorescence in the lumen of the developing gastrointestinal tract. PED6 was added to zebrafish embryos at 5 dpf

followed by imaging the fish at 6 dpf with the average fluorescence emission at 540 nm excitation at 505 nm. Images were taken at 6 dpf using a Leica microscope and analyzed using the ImageJ software.

Histopathology and Evaluation of Tissue Morphology

Zebrafish embryos were evaluated histopathologically for morphologic alterations induced by radiation exposure and potential radioprotective effects of EP and CDDO-TFEA with special emphasis on the gastrointestinal morphology. Briefly, embryos at 24 hpf were exposed to 0 or 12 Gy in the presence or absence of either CDDO-TFEA or EP administered 1 h prior to ionizing radiation. Embryos were sacrificed, fixed by immersion in 4 % paraformaldehyde for 24 h, and then rinsed and placed in 10× PBS for another 24 h. Sections were embedded in paraffin, and coronal, transverse, and sagittal whole-body sections (4 µm thickness) were generated. All sections were stained with H&E, mounted on glass slides, and examined by light microscope; representative images were taken using a QIMAGING camera and iVision software.

NF-κB Reporter Assay

NF-κB reporter assay was done as described by us previously [22] with minor modifications. HeLa cells were seeded at 7.5×10^4/mL in DMEM supplemented with 10% fetal bovine serum. The cells were cotransfected with the pSEAP2-NF-κB vector (BDBioSciences) encoding a secreted form of human placental alkaline phosphatase driven by a NF-κB–responsive promoter and a β-galactosidase expression vector for control purposes. Forty-eight hours posttransfection, different NF-κB inhibitors (0.5 µmol/L velcade, 5 µmol/L MG-132, 1 mmol/L EP, 1 µmol/L CDDO) were added to the cells in serum-free media for 24 h. NF-κB–dependent transcription in the absence and presence of recombinant TNF-α (10 ng/mL; R&DSystems) was determined 72 h posttransfection using the Great EscAPe SEAP Reporter System 3, which is based on detection of secreted alkaline phosphatase in cell supernatants normalized to β-galactosidase activity using the luminescent β-gal detection kit (BDBiosciences).

Reverse Transcription PCR Analysis

Zebrafish total RNA was isolated from 100 embryos per experimental condition at 30 hpf (6 h post radiation) using the RNeasy mini kit (QIAGEN Sciences) and stored at −80°C. For reverse transcription, total RNA was annealed with Oligo(dT) primer (Roche) at 70°C for 5 min followed by the incubation at 42°C for 1 h. Reverse transcription reaction products were boiled for 2 min followed by incubation on ice for 2 min before use. Primer sequences used for amplification of *bax*, *mdm2*, *p21/waf-1*, and *β-actin* zebrafish sequences are provided in Supplementary Table S1. PCR reaction conditions were 94°C, 60°C, 72°C for 30 s, 30 s, 1 min, respectively, and 35 cycles with 7 min extension time after the last cycle. Thermo Fisher Scientific Taq-polymerase was used in 50 µL PCR reaction mix containing 1 µL reverse transcription reaction. PCR reactions were analyzed by 1.5% agarose gel electrophoresis.

Statistical Analysis

All experiments were done at least three times with at least 75 embryos total per experimental group. To determine statistically significant differences between groups χ^2 tests were done.

Results

Proteasome Inhibitors Radiosensitize Zebrafish Embryos

The proteasome inhibitor PS-341 (Bortezomib/VELCADE) is presently the only Food and Drug Administration–approved drug with well-characterized inhibitory effects on NF-κB activity.[18] PS-341 is a small, cell-permeable molecule inhibiting proteasome activity in a reversible manner. In addition to reducing the activation state of NF-κB by inhibiting proteasomal degradation of IκB, PS-341 affects many other pathways and targets, leading to high expression levels of several proapoptotic proteins in certain experimental conditions.[23] *In vitro*, PS-341 has been found to enhance antitumor cell effects of select chemotherapeutic agents[6,24], tumor cell targeting antibodies[25], and ionizing radiation[26]. Yet, little is known about the combined effects of PS-341 and ionizing radiation on normal cells and tissues of vertebrate organisms. To address this issue we used PS-341 in zebrafish embryos exposed to high doses of ionizing radiation as described by us previously.[4, 27, 28] We first established that treatment of zebrafish with PS-341 alone (dose range, 0–10 µmol/L) was nontoxic as assessed by embryo survival and gross morphology during the first 7 days after fertilization (Supplementary Fig. S1). In contrast, PS-341 (1 µmol/L) markedly sensitized zebrafish embryos to the lethal effects of ionizing radiation when administered 1 hour prior to radiation (Fig. 1A). In these experiments zebrafish embryos were exposed at 24 hpf to 20 Gy, previously determined to kill 50% of irradiated zebrafish embryos by day 7 of development.[27] In HeLa cells, at the same concentration (1 µmol/L) PS-341 abrogated the TNF-α–induced NF-κB activity, whereas it did not significantly affect the basal activity (Supplementary Fig. 2A and B).

To ascertain whether radiation sensitization by PS-341 could be replicated using other inhibitors of the proteasome we next tested the effects of MG132, a nonboronated small molecule inhibitor of the 26S proteasome,[29] on zebrafish survival in the presence and absence of ionizing radiation. Similar to PS-341, MG132 was remarkably nontoxic when applied as a single agent to zebrafish embryos (dose range, 0–50 µmol/L) yet efficiently inhibited TNF-α–induced but not the baseline NF-κB activity in HeLa cells when used at 5 µmol/L (Supplementary Fig. 2A and B). At this concentration, however, MG132 marginally sensitized zebrafish embryos to the lethal effects of 20 Gy ionizing radiation albeit to a lesser degree than PS-341 (Fig. 1B). An irreversible proteasome inhibitor (lactacystin) at a nontoxic concentration (5 µmol/L) also slightly radiosensitized zebrafish embryos in a manner similar to MG132 (Fig. 1C).

These results show that several proteasome inhibitors do not protect normal cells and tissues in the developing fish larvae against the deleterious effects of radiation. As p53 is a major target of proteasomal degradation and enhances ionizing radiation–associated tissue damage in mice[30–32] and zebrafish[33, 34] we asked whether the deleterious effects of proteasome inhibitors could be linked to p53 stabilization and subsequent induction of target genes. Consistent with our earlier observations, ablating p53 expression by antisense morpholino oligodeoxynucleotide[35] or p53 function by PFT-α (1 µmol/L) given to zebrafish embryos at 24 hpf[34] markedly improved zebrafish survival after radiation either alone or in combination with PS-341 (not shown). However, reverse transcription-PCR analysis did not reveal increased steady-state mRNA levels of the p53 targets *p21/WAF1*, *bax*, or the zebrafish ortholog of *mdm2* in PS-341–treated embryos whereas ionizing radiation led, as expected, to elevated transcript levels for these genes (Supplementary Fig. S3). Thus, the molecular target(s) responsible for radiosensitization by PS-341 and their relationship, if any, to the p53 response remain to be identified.

Radiation Protection of Zebrafish Embryos by the NF-κBp65 Inhibitor Ethyl Pyruvate

In consideration of the fact that proteasome inhibitors affect multiple intracellular pathways in addition to NF-κB and to pinpoint the functional contribution of NF-κB to the radiation response of zebrafish embryos, we tested the effects of a series of pharmacologic inhibitors of NF-κB activity with different mechanisms of action on the radiation response of zebrafish embryos. Reducing NF-κB activity by expression of upstream regulator

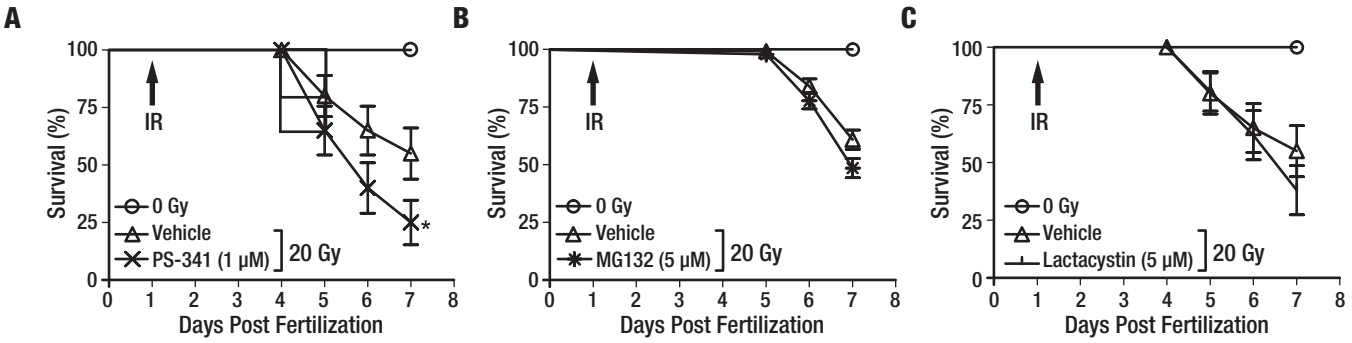

Figure 1. Effects of the proteasome inhibitors PS-341 (**A**), MG132 (**B**), and lactacystin (**C**) on the radiation sensitivity of zebrafish embryos. Embryos were irradiated at 24 hpf and survival was scored every day up to 7 dpf. Results shown represent mean ± SD of triplicate experiments. *, statistically significant difference in survival at 6 to 7 dpf.

IκB has previously been shown to cause severe embryonal malformations in zebrafish[36, 37] and, thus, was not further considered. In addition, knockdown of the NF-κBp65 subunit by antisense morpholinos similarly caused severe morphologic defects (no tail phenotype) during the first 3 days of development (Supplementary Fig. S4) consistent with published results[37] and, thus, was not informative in the context of assaying the radiation response. Instead, we used pharmacologic inhibitors that disrupt the canonical pathway to NF-κB activation and could be used at concentrations that do not interfere with embryonal development. First, we tested EP, a ROS scavenger and inhibitor of NF-κBp65[38]. EP inhibits the DNA binding activity of NF-κBp65 by binding to a reactive cysteine in the DNA binding site (Cys 38) of NF-κBp65[13], which is shared between humans and zebrafish (Supplementary Fig. S2C). EP has very recently been shown to mitigate deleterious effects of total body irradiation in mice[12]. We observed that EP similarly not only protected against but also mitigated lethality associated with whole body irradiation of zebrafish embryos (Fig. 2A, C, and F). EP was administered at various time points ranging from 1 hour prior to radiation exposure to 3 hours postirradiation. The ROS scavengers amifostine and DF-1 served as positive controls in these experiments as we observed marked protection of embryos by these two compounds in earlier work.[4, 27] Whereas amifostine and DF-1 afforded protection against deleterious effects of ionizing radiation when administered prior to or concurrent with radiation, neither compound could mitigate the lethal effects of radiation when given beyond 15 minutes after ionizing radiation[27]. In marked contrast, EP administered up to 2 hours after radiation significantly reduced ionizing radiation–associated lethality (Fig. 2F).

The IKK Inhibitor CDDO-TFEA Mitigates Radiation Effects in Zebrafish Embryos

To further address the relevance of NF-κB activation in modulating radiation sensitivity of zebrafish embryos we used CDDO-TFEA that inhibits NF-κB signaling by interacting with Cys179 of IKKβ, inhibiting its activity and preventing phosphorylation and proteasomal degradation of IκB[39] and, thus, through a molecular mechanism distinct from EP. The amino acid sequence around this reactive Cys179 is also highly conserved in zebrafish (Supplementary Fig. 2C). CDDO-TFEA protected against and mitigated overall lethal effects of radiation in zebrafish embryos in a manner similar to EP (Fig. 2B, D , and F). We next determined whether mitigation of radiation effects cosegregated with the capacity of the compounds under investigation to act as ROS scavengers. This was based on the findings that, in addition to directly binding to IKKβ, CDDO has been described to induce expression of enzymes catalyzing antioxidant reactions in peripheral blood mononuclear cells due to increased nuclear accumulation of Nrf2, an oxidant-responsive bZIP transcription factor.[40, 41] Whereas EP is an effective ROS scavenger in irradiated zebrafish embryos, CDDO-TFEA did not reduce ROS levels measured 2 hours after radiation exposure (Supplementary Fig. S5). Thus, at least the effect of CDDO-TFEA on radiation mitigation cannot be ascribed to ROS scavenging, whereas in the case of EP, ROS scavenging and NF-κB inhibition may be jointly responsible for the beneficial effects of EP in the mitigation setting. Of note, the ROS scavengers with no known effect on NF-κB signal transduction (amifostine and DF-1) do not mitigate radiation effects if administered beyond 15 minutes after ionizing radiation.[27] To further probe whether IKK inhibition is radioprotective we tested four additional small molecule IKK inhibitors, i.e. Wedelolactone (IKK inhibitor 2), BMS-345541 (IKK inhibitor 3) and IKK-2 inhibitors 4 and 5. All four agents protected zebrafish embryos against the lethal effects of radiation in a manner similar to CDDO-TFEA and EP (Fig. 2E). Moreover, unlike EP or CDDO-TFEA, these agents are not known to have antioxidant properties and primarily inhibit IκBα phosphorylation by IKKβ (i.e., IKK-2). On balance, these results suggest that prolonged and excessive activation of the canonical NF-κB pathway is a major contributor to radiation toxicity in the developing vertebrate organism and that inhibiting this pathway may protect the organism against deleterious effects of radiation.

Organ-Specific Radiation Protection by CDDO-TFEA and EP

Having established that EP and CDDO-TFEA provide whole-body protection against lethal doses of radiation and in consideration of the fact that these compounds are in preclinical development, we next determined organ-specific radiation protective effects of these two NF-κB inhibitors. First, we assessed, by acridine orange staining, organism-wide apoptosis in zebrafish embryos determined 6 hours after radiation. Consistent with earlier reports [33], we observed increased acridine orange staining in the central nervous system and along the body axis of irradiated embryos. Both NF-κB inhibitors markedly reduced radiation-induced acridine orange staining (Fig. 3). We previously reported that ionizing radiation compromised zebrafish kidney function as determined by delayed excretion of a fluorescent dextran injected intracardially.[27] Treatment with EP but not CDDO-TFEA significantly reversed the effect of ionizing radiation on dextran clearance of irradiated embryos to near normal levels, suggesting protection against ionizing radiation–induced kidney damage (Fig. 4). It is currently unknown whether this effect reflects differences in ROS scavenging capacity between the two compounds as described

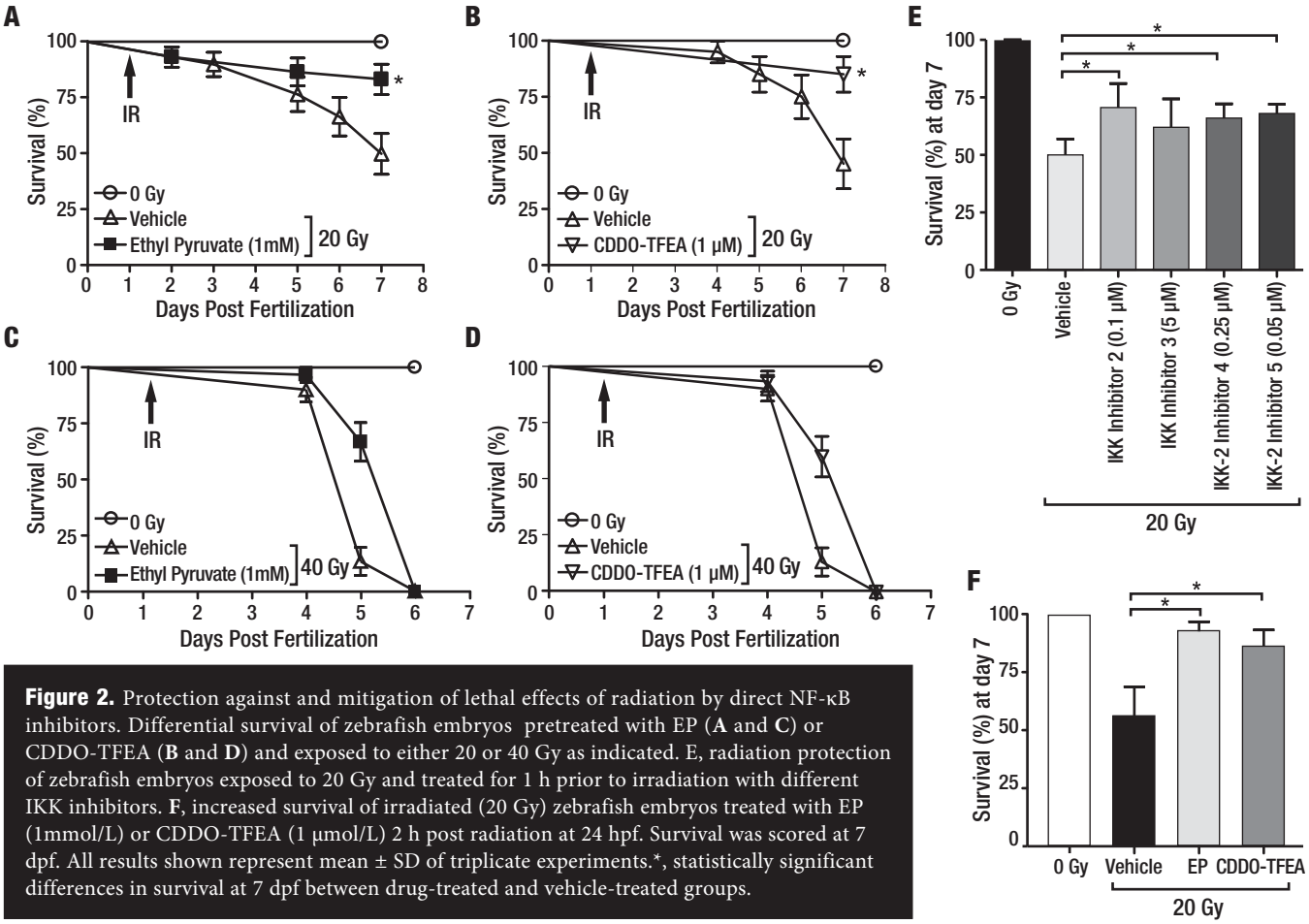

Figure 2. Protection against and mitigation of lethal effects of radiation by direct NF-κB inhibitors. Differential survival of zebrafish embryos pretreated with EP (**A** and **C**) or CDDO-TFEA (**B** and **D**) and exposed to either 20 or 40 Gy as indicated. E, radiation protection of zebrafish embryos exposed to 20 Gy and treated for 1 h prior to irradiation with different IKK inhibitors. **F**, increased survival of irradiated (20 Gy) zebrafish embryos treated with EP (1mmol/L) or CDDO-TFEA (1 μmol/L) 2 h post radiation at 24 hpf. Survival was scored at 7 dpf. All results shown represent mean ± SD of triplicate experiments.*, statistically significant differences in survival at 7 dpf between drug-treated and vehicle-treated groups.

above (Supplementary Fig. S5) or is due to differences in pharmacokinetics or pharmacodynamics. In addition, radiation of zebrafish embryos is associated with a high incidence of a body axis malformation called "curly-up" to describe aberrant dorsal curvature of the fish tail. Both CDDO-TFEA and EP reduced the incidence of curly-up significantly (Fig. 5).

Finally, we determined the effects of radiation on the developing gastrointestinal system. This was done in consideration of several prior reports suggesting that NF-κB activation protects the gastrointestinal tract of higher vertebrates against acute radiation damage.[42, 43] Radiation protection of the gastrointestinal system was determined in several ways. First, we assayed overall gastrointestinal function by scoring "long-term" survival of fish irradiated in the presence and absence of EP or CDDO-TFEA (up to 15 dpf). Fish larvae become dependent on external food sources at approximately 6 dpf when the contents of the yolk sac are depleted. Significant functional damage to the gastrointestinal system will thus lead to death by starvation within 10 days after conception.[19] Conversely, survival of fish beyond two weeks indicates establishment of a functionally adequate gastrointestinal system. Both EP and CDDO-TFEA increased extended survival of zebrafish larvae (Supplementary Fig. S6) although this effect was statistically significant only in the case of CDDO-TFEA. To address the combined effects of radiation and EP or CDDO-TFEA treatment on the developing gastrointestinal system further, we determined gastrointestinal lumen formation by use of a fluorescent reporter (PED6; ref. 21) that is metabolized and excreted through the gastrointestinal system. This analysis revealed severely impaired lumen formation of the gastrointestinal system induced by ionizing radiation (15 Gy) and partial restoration of lumen formation and fluorescent dye excretion by treatment with either EP or CDDO. These functional results were complemented by examining the histologic appearance of the gastrointestinal system 5 days after radiation exposure in the presence and absence of the NF-κB inhibitors under investigation (Fig. 6). The hindgut mucosal epithelium immediately proximal to the cloaca revealed distinct cellular changes associated with sublethal ionizing radiation exposure (12 Gy), including irregular shape and disorganization of the columnar absorbing cells with redistribution of nuclei away from the basal orientation. In addition, decreased goblet cell numbers were observed. By contrast, EP and CDDO-TFEA pretreatment of irradiated embryos restored, in part, the columnar structure of absorbing cells and basal location of nuclei.

Discussion

Our results show that 6 of 6 pharmacologic inhibitors with different chemical structures and mode of actions inhibit the canonical pathway of NF-κB activation (consisting of IKKβ/IκB/NF-κBp65) and provide protection against radiation-induced overall lethality and damage to multiple organ systems of the developing zebrafish. By contrast, 3 of 3 proteasome inhibitors did not afford radiation protection, but radiosensitized zebrafish embryos to the lethal effects of ionizing radiation.

Taking into account that each of the pharmacologic agents used in this study is likely to affect targets other than NF-κB, it is remarkable that radioprotection cosegregated with interference with activation of the canonical pathway to NF-κB. This observation suggests that NF-κB may be the relevant target for radiation protection by pharmacologic IKK/NF-κB inhibition.

Currently, there is no consensus about the functional contribution of NF-κB activation to the radiation response.[44] Abundant reports of radiosensitization of tumor cells *in vitro* and *in vivo* by NF-κB inhibition are contrasted by relatively few such reports dealing with normal cells. The use of genetically engineered mouse models to monitor NF-κB dysfunction in normal tissues has been limited due to embryonal lethality observed in IKKβ[45] and NF-κBp65[46] knockout animals. In cases where either conditional knockouts were made or transgenic mice were generated by forced expression of dominant negative regulators to modulate NF-κB activation, the interpretation of results is further complicated by compensatory adjustments of homeostasis (for review see ref. 47). The present study sidesteps the problems inherent to using genetic models by examining the effects of pharmacologic agents used at concentrations that reduce but do not abrogate NF-κB activity. The ease of our "assay system," i.e., observation of overall effects of ionizing radiation on zebrafish survival as well as effects on specific target organs, allowed us to monitor the effects of drug classes grouped according to target specificity and mechanisms of action. This approach had the advantage to minimize confounding effects due to unknown, off-target effects of any pharmacologic agent. By contrast, and as expected, ablating NF-κB activity by targeting IKKβ or NF-κBp65 expression using antisense approaches produced a dramatically different outcome as these

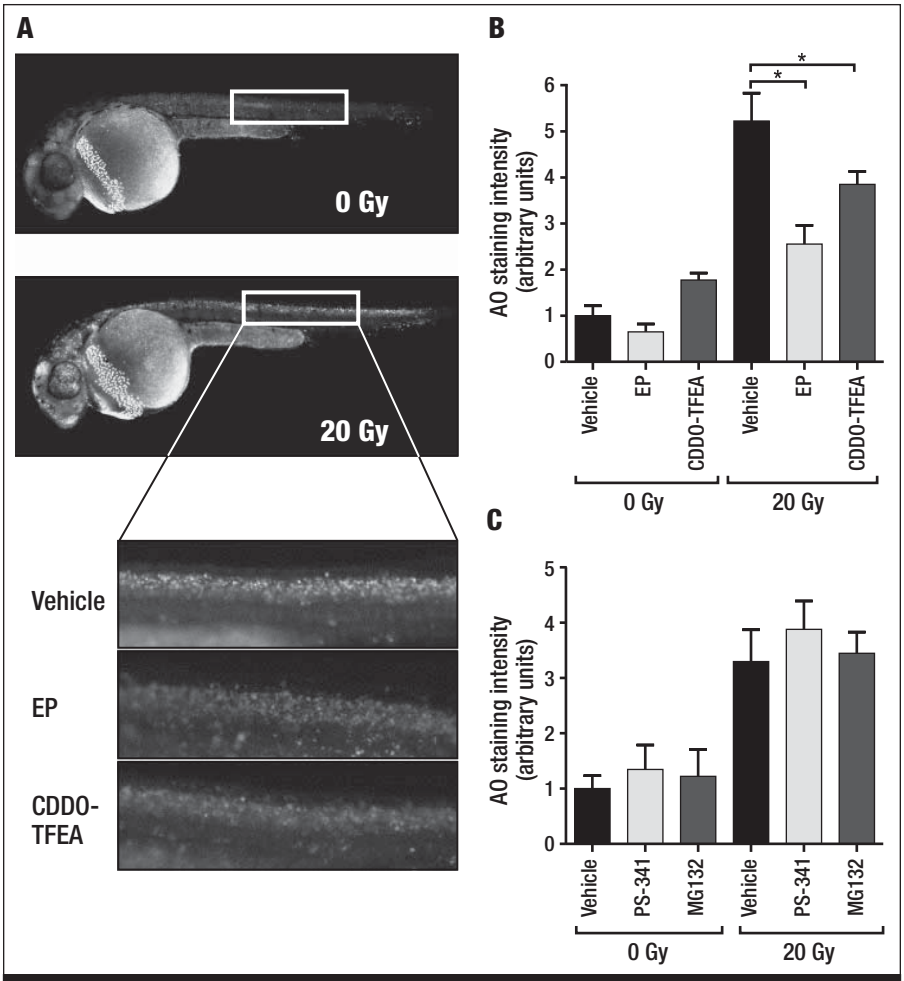

Figure 3. Reduction of organism-wide apoptosis by EP and CDDO-TFEA treatment preradiation and postradiation. Acridine orange (AO) staining of whole embryos was done 6 h postradiation at 30 hpf. **A**, representative examples of control or irradiated fish revealing strong AO staining in the central nervous system and along the body axis induced by radiation (20 Gy). Regions selected for quantitative evaluation are boxed. **B**, reduced AO staining in CDDO-TFEA- and EP-treated embryos exposed to ionizing radiation. **C**, PS-341 or MG132 treatment does not significantly affect AO staining of embryos exposed to ionizing radiation.

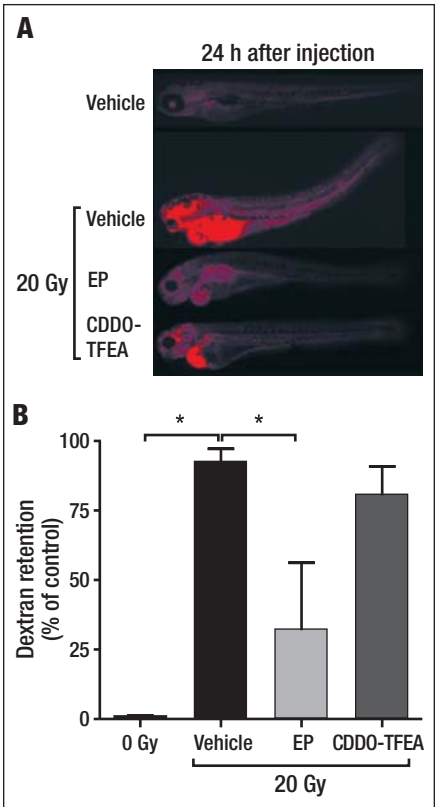

Figure 4. Effects of EP and CDDO-TFEA on radiation-induced kidney damage as determined by dextran clearance. **A**, Representative images of dextran retention in irradiated embryos and effects of EP and CDDO-TFEA on this phenomenon. **B**, quantitative representation of dextran retention in embryos treated with either EP or CDDO-TFEA as indicated; results are expressed relative to vehicle-treated, nonirradiated controls. *, statistically significant differences between the experimental groups indicated by brackets.

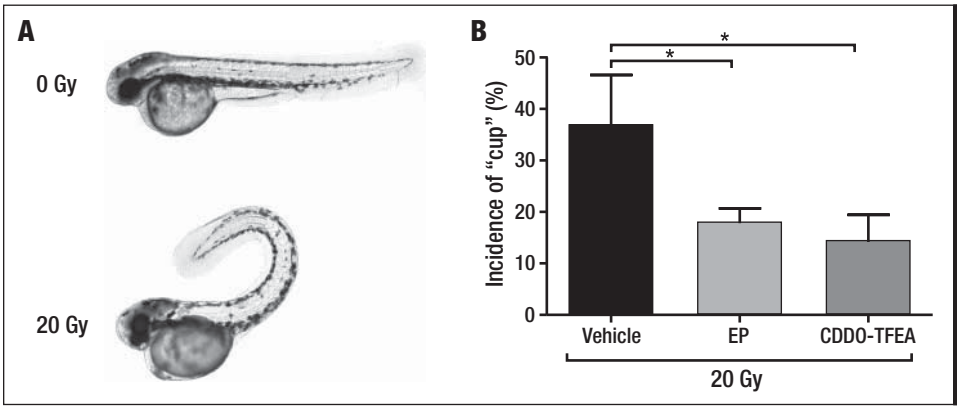

Figure 5. EP and CDDO-TFEA alleviate radiation-induced malformations of the body axis. **A**, representative micrographs showing dorsal curvature ("curly-up"; *cup*) in irradiated (20 Gy) embryos at 72 hpf relative to control nonirradiated fish embryos. **B**, quantification of curly-up incidence in CDDO-TFEA- and EP-treated fish relative to vehicle-treated controls. *, statistically significant differences between the experimental groups indicated by brackets.

interventions were associated with embryonic lethality even in the absence of genotoxic stress (see Supplementary Fig. S4 and ref. 46). This result is consistent with the view that inhibition of excess NF-κB activity after lethal irradiation is beneficial whereas blocking NF-κB expression and/or activation altogether, as in genetic knockout/knockdown models, is deleterious (even in the absence of radiation). This contention is further supported by our finding that EP and CDDO-TFEA at the nontoxic concentration used here disrupted TNF-α–induced NF-κB activation but not basal NF-κB activity in HeLa cells *in vitro* (Supplementary Fig. S2). Importantly, CDDO-TFEA and EP not only protected against but also mitigated the lethal effects of radiation. This result is of interest as it points to the importance of sustained NF-κB activation consistent with inflammatory responses rather than the burst of NF-κB activity observed immediately after radiation exposure. It remains to be seen whether other anti-inflammatory agents may be used to mitigate radiation damage to normal tissues in the developing embryo.

Interestingly, radiation protection of zebrafish embryos by NF-κB inhibitors extended to the gastrointestinal system whereas previous work using genetically modified mice[42] and the TLR5 ligand flagellin[43] has implicated NF-κB activation in radiation protection of gastrointestinal stem cells. The reason(s) for this difference are unclear at this point. However, the TLR5 ligand flagellin exerts pleiotropic stimulatory effects on multiple signaling pathways that include NF-κB but also p38, Erk/mitogen-activated protein kinase, and potentially, signal transducers and activators of transcription.[48] It has not been reported which of these multiple effects alone or in combination is at cause for radioprotection provided by flagellin.[43] In addition, the NF-κB inhibitory effects of both EP and CDDO-TFEA are completely reversible, whereas genetic ablation is not and this circumstance could affect outcomes of NF-κB activation in reference to gastrointestinal function. Our findings are further consistent with the view that excessive NF-κB activation, as observed in the context of chronic inflammation, is potentially deleterious to the gastrointestinal system[49] and, thus, down-modulating NF-κB activity but not ablating it altogether can be advantageous in certain settings.[50] Although the details of these diverse outcomes in different model systems remain to be sorted out, our results clearly show that reducing NF-κB activity with a variety of compounds with different mechanisms of action diminishes radiation-induced damage to several organ systems in the developing zebrafish embryo.

In conclusion, the most salient finding of this study is that direct inhibitors of NF-κB activity provided effective protection and mitigation against overall lethality and specific organ damage caused by ionizing radiation in zebrafish embryos. Direct NF-κB inhibitors also exert antineoplastic effects in select model systems as shown extensively for CDDO-TFEA and derivatives thereof.[51–57] These findings are consistent with a favorable therapeutic window for NF-κB inhibitors when used in combination with radiation and, potentially, chemotherapeutic drugs.

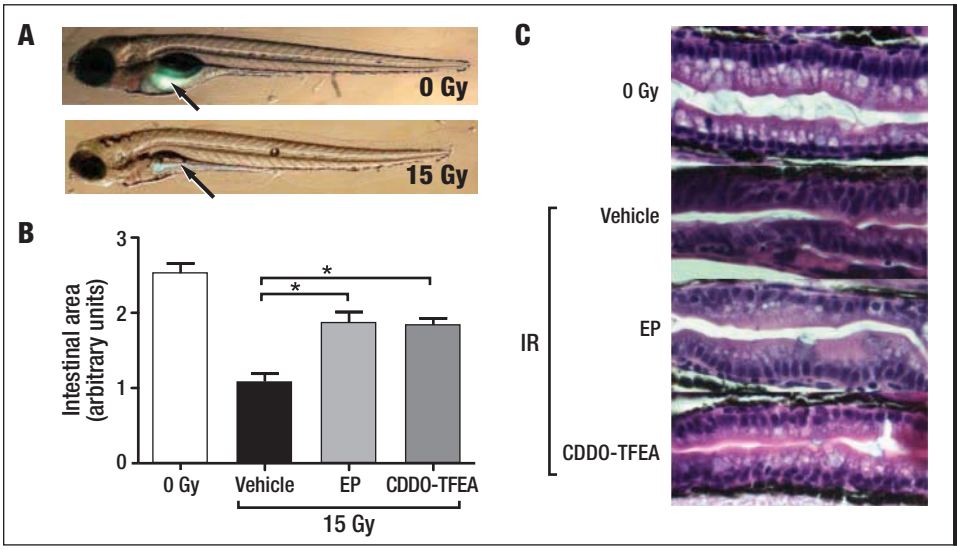

Figure 6. Effects of EP and CDDO-TFEA on radiation-induced alterations of the gastrointestinal system. **A**, improved PLA_2 activity and gastrointestinal lumen formation in irradiated zebrafish treated with either EP or CDDO-TFEA. Dequenched fluorescence reflects endogenous PLA_2 activity and transport of cleavage products through the lumen of the developing gastrointestinal system. **B**, quantitative evaluation of gastrointestinal lumen formation as determined by fluorescent dye content at 6 dpf. **C**, representative histologic sections of hindgut proximal to the cloaca at 6 dpf [5 d post (12 Gy)].

Disclosure of Potential Conflicts of Interest

No potential conflicts of interest were disclosed.

Acknowledgments

We gratefully acknowledge the support of the Zebrafish Core Facility at the Department of Biochemistry and Molecular Biology, Thomas Jefferson University.

References

1. Sonis ST. The pathobiology of mucositis. *Nat Rev Cancer* 2004;4:277–284.
2. Hall PD, Benko H, Hogan KR, Stuart RK. The influence of serum tumor necrosis factor-α and interleukin-6 concentrations on nonhematologic toxicity and hematologic recovery in patients with acute myelogenous leukemia. *Exp Hematol* 1995;23:1256–60.
3. Stone HB, Moulder JE, Coleman CN, *et al.* Models for evaluating agents intended for the prophylaxis, mitigation and treatment of radiation injuries. Report of an NCI Workshop, December 3–4, 2003. *Radiat Res* 2004;162:711–28.
4. McAleer MF, Davidson C, Davidson WR, *et al.* Novel use of zebrafish as a vertebrate model to screen radiation protectors and sensitizers. *Int J Radiat Oncol Biol Phys* 2005;61:10–3.
5. Ghosh S, Hayden MS. New regulators of NF-κB in inflammation. *Nat Rev Immunol* 2008;8:837–48.
6. Cusack JC, Jr., Liu R, Houston M, *et al.* Enhanced chemosensitivity to CPT-11 with proteasome inhibitor PS-341: implications for systemic nuclear factor-κB inhibition. *Cancer Res* 2001;61:3535–40.
7. Braunstein S, Formenti SC, Schneider RJ. Acquisition of stable inducible up-regulation of nuclear factor-κB by tumor necrosis factor exposure confers increased radiation resistance without increased transformation in breast cancer cells. *Mol Cancer Res: MCR* 2008;6:78–88.
8. Ahmed KM, Li JJ . ATM-NF-κB connection as a target for tumor radiosensitization. *Curr Cancer Drug Targets* 2007;7:335–42.
9. Kim BY, Kim KA, Kwon O, et al. NF-κB inhibition radiosensitizes Ki-Ras-transformed cells to ionizing radiation. *Carcinogenesis* 2005;26:1395–403.
10. Munshi A, Kurland JF, Nishikawa T, Chiao PJ, Andreeff M, Meyn RE. Inhibition of constitutively activated nuclear factor-κB radiosensitizes human melanoma cells. *Mol Cancer Ther* 2004;3:985–92.
11. Meyer CJ, Sporn MB, Wigley WC, Sonis ST. RAT 402 (CDDO-Me) suppresses tumor and treatment induced inflammation, sensitizing tumors to and protecting normal tissue from radiation. *Eur J Cancer* 2006;4:162.
12. Epperly M, Jin S, Nie S, *et al.* Ethyl pyruvate, a potentially effective mitigator of damage after total-body irradiation. *Radiat Res* 2007;168:552–9.
13. Han Y, Englert JA, Yang R, Delude RL, Fink MP. Ethyl pyruvate inhibits nuclear factor-κB–dependent signaling by directly targeting p65. *J Pharmacol Exp Ther* 2005;312:1097–105.
14. Shishodia S, Sethi G, Konopleva M, Andreeff M, Aggarwal BB. A synthetic triterpenoid, CDDO-Me, inhibits IκBα kinase and enhances apoptosis induced by TNF and chemotherapeutic agents through down-regulation of expression of nuclear factor κB–regulated gene products in human leukemic cells. *Clin Cancer Res* 2006;12:1828–38.
15. Liby K, Voong N, Williams CR, *et al.* The synthetic triterpenoid CDDOImidazolide suppresses STAT phosphorylation and induces apoptosis in myeloma and lung cancer cells. *Clin Cancer Res* 2006;12:4288–93.
16. Ahmad R, Raina D, Meyer C, Kufe D. Triterpenoid CDDO-methyl ester inhibits the Janus-activated kinase-1 (JAK1)->signal transducer and activator of transcription-3 (STAT3) pathway by direct inhibition of JAK1 and STAT3. *Cancer Res* 2008;68:2920–6.
17. Perkins ND, Gilmore TD. Good cop, bad cop: the different faces of NF-κB. *Cell Death Differ* 2006;13:759–72.
18. Zavrski I, Kleeberg L, Kaiser M, *et al.* Proteasome as an emerging therapeutic target in cancer. *Curr Pharm Des* 2007;13:471–85.
19. Westerfield M. *The zebrafish book.* Eugene OR: University of Oregon Press; 1995.
20. Hentschel DM, Park KM, Cilenti L, Zervos AS, Drummond I, Bonventre JV. Acute renal failure in zebrafish: a novel system to study a complex disease. *Am J Physiol- Renal Fluid Electrolyte Physiol* 2005;288:F923–9.
21. Farber SA, Pack M, Ho SY, *et al.* Genetic analysis of digestive physiology using fluorescent phospholipid reporters. *Science* 2001;292:1385–8.
22. Ren Q, Kari C, Quadros MR, *et al.* Malignant transformation of immortalized HaCaT keratinocytes through deregulated nuclear factor κB signaling. *Cancer Res* 2006;66:5209–15.
23. Milano A, Iaffaioli RV, Caponigro F. The proteasome: a worthwhile target for the treatment of solid tumours? *Eur J Cancer* 2007;43:1125–33.
24. Neukirchen J, Meier A, Rohrbeck A, *et al.* The proteasome inhibitor bortezomib acts differently in combination with p53 gene transfer or cytotoxic chemotherapy on NSCLC cells. *Cancer Gene Ther* 2007;14:431–9.
25. Cardoso F, Durbecq V, Laes J-F, *et al.* Bortezomib (PS-341, Velcade) increases the efficacy of trastuzumab (Herceptin) in HER-2–positive breast cancer cells in a synergistic manner. *Mol Cancer* Ther 2006;5:3042–51.
26. Russo SM, Tepper JE, Baldwin AS, Jr., *et al.* Enhancement of radiosensitivity by proteasome inhibition: implications for a role of NF-κB. *Int J Radiat Oncol Biol Phys* 2001;50:183–93.
27. Daroczi B, Kari G, McAleer MF, Wolf JC, Rodeck U, Dicker AP. In vivo radioprotection by the fullerene nanoparticle DF-1 as assessed in a zebrafish model. *Clin Cancer Res* 2006;12:7086–91.
28. McAleer MF, Duffy KT, Davidson WR, *et al.* Antisense inhibition of cyclin D1 expression is equivalent to flavopiridol for radiosensitization of zebrafish embryos. *Int J Radiat Oncol Biol Phys* 2006;66:546–51.
29. Rock KL, Gramm C, Rothstein L, *et al.* Inhibitors of the proteasome block the degradation of most cell proteins and the generation of peptides presented on MHCclass I molecules. *Cell* 1994;78:761–71.
30. Komarov PG, Komarova EA, Kondratov RV, *et al.* A chemical inhibitor of p53 that protects mice from the side effects of cancer therapy. *Science* 1999;285:1733–7.
31. Komarova EA, Christov K, Faerman AI, Gudkov AV. Different impact of p53 and p21 on the radiation response of mouse tissues. *Oncogene* 2000;19:3791–8.
32. Komarova EA, Kondratov RV,Wang K, *et al.*Dual effect of p53 on radiation sensitivity in vivo: p53 promotes hematopoietic injury, but protects from gastro-intestinal syndrome in mice. *Oncogene* 2004;23:3265–71.
33. Berghmans S, Murphey RD, Wienholds E, *et al.* tp53 mutant zebrafish develop malignant peripheral nerve sheath tumors. *Proc Natl Acad Sci U S A* 2005;102:407–12.
34. Davidson W, Ren Q, Kari G, Kashi O, Dicker AP, Rodeck U. Inhibition of p73 function by Pifithrin-α as revealed by studies in zebrafish embryos. *Cell Cycle* 2008;7:1224–30.
35. Langheinrich U, Hennen E, Stott G, Vacun G. Zebrafish as a model organism for the identification and characterization of drugs and genes affecting p53 signaling. *Curr Biol* 2002;12:2023–8.
36. Correa RG, Matsui T, Tergaonkar V, Rodriguez-Esteban C, Izpisua- Belmonte JC , Verma IM. Zebrafish IκB kinase 1 negatively regulates NF-κB activity. *Curr Biol* 2005;15:1291–5.
37. Correa RG, Tergaonkar V, Ng JK, Dubova I, Izpisua-Belmonte JC, Verma IM. Characterization of NF-κ B/I κ B proteins in zebra fish and their involvement in notochord development. *Mol Cell Biol* 2004;24:5257–68.
38. Fink MP. Ethyl pyruvate: a novel anti-inflammatory agent. *J Intern Med* 2007;261:349–62.
39. Yore MM, Liby KT, Honda T, Gribble GW, Sporn MB. The synthetic triterpenoid 1-[2-cyano-3,12-dioxooleana-1,9(11)-dien-28-oyl]imidazole blocks nuclear factor-κB activation through direct inhibition of IκB kinase β. *Mol Cancer Ther* 2006;5:3232–9.
40. Thimmulappa RK, Fuchs RJ, Malhotra D, *et al.* Preclinical evaluation of targeting the Nrf2 pathway by triterpenoids (CDDO-Im and CDDO-Me) for protection from LPS-induced inflammatory response and reactive oxygen species in human peripheral blood mononuclear cells and neutrophils. *Antioxid Redox Signal* 2007;9:1963–70.
41. Yates MS, Tauchi M, Katsuoka F, *et al.* Pharmacodynamic characterization of chemopreventive triterpenoids as exceptionally potent inducers of Nrf2-regulated genes. *Mol Cancer Ther* 2007;6:154–62.
42. Egan LJ, Eckmann L, Greten FR, *et al.* IκB-kinaseβ-dependent NF-κB activation provides radioprotection to the intestinal epithelium. *Proc Natl Acad Sci U S A* 2004;101:2452–7.
43. Burdelya LG, Krivokrysenko VI, Tallant TC, *et al.* An agonist of toll-like receptor 5 has radioprotective activity in mouse and primate models. *Science* 2008;320:226–30.
44. Janssens S, Tschopp J. Signals from within: the DNA-damage-induced NF-κB response. *Cell Death Differ* 2006;13:773–84.
45. Li Q, Van Antwerp D, Mercurio F, Lee KF, Verma IM. Severe liver degeneration in mice lacking the IκB kinase 2 gene. *Science* 1999;284:321–5.
46. Beg AA, Sha WC, Bronson RT, Ghosh S, Baltimore D. Embryonic lethality and liver degeneration in mice lacking the RelA component of NF-κ B. *Nature* 1995;376:167–70.
47. Gerondakis S, Grumont R, Gugasyan R, *et al.* Unravelling the complexities of the NF-κB signalling pathway using mouse knockout and transgenic models. *Oncogene* 2006;25:6781–99.
48. Vijay-Kumar M, Gewirtz AT. Guardians of the gut: newly appreciated role of epithelial toll-like receptors in protecting the intestine. [comment]. *Gastroenterology* 2008;135:351–4.
49. Eckmann L, Nebelsiek T, Fingerle AA, *et al.* Opposing functions of IKKβ during acute and chronic intestinal inflammation. *Proc Natl Acad Sci U S A* 2008;105:15058–63.
50. Groesdonk HV, Senftleben U. Modulation of inhibitor κB kinase/nuclear factor κB signaling during critical illness: a double-edged sword. [comment]. *Crit Care Med* 2004;32:1239; author reply 1239–1240.
51. Gao X, Deeb D, Jiang H, Liu Y, Dulchavsky SA, Gautam SC. Synthetic triterpenoids inhibit growth and induce apoptosis in human glioblastoma and neuroblastoma cells through inhibition of prosurvival Akt, NF-κB and Notch1 signaling. *J Neurooncol* 2007;84:147–57.
52. Kress CL, Konopleva M, Martinez-Garcia V, *et al.* Triterpenoids display single agent anti-tumor activity in a transgenic mouse model of chronic lymphocytic leukemia and small B cell lymphoma. *PLoS ONE* [Electronic Resource] 2007;2:e559.
53. Hyer ML, Croxton R, Krajewska M, *et al.* Synthetic triterpenoids cooperate with tumor necrosis factor-related apoptosis-inducing ligand to induce apoptosis of breast cancer cells. *Cancer Res* 2005;65:4799–808.
54. Chauhan D, Li G, Podar K, et al. The bortezomib/proteasome inhibitor PS-341 and triterpenoid CDDO-Im induce synergistic anti-multiple myeloma (MM) activity and overcome bortezomib resistance. Blood 2004;103:3158–66.
55. Place AE, Suh N, Williams CR, et al. The novel synthetic triterpenoid, CDDO-imidazolide, inhibits inflammatory response and tumor growth in vivo. Clin Cancer Res 2003;9:2798–806.
56. Ito Y, Pandey P, Sporn MB, Datta R, Kharbanda S, Kufe D. The novel triterpenoid CDDO induces apoptosis and differentiation of human osteosarcoma cells by a caspase-8 dependent mechanism. Mol Pharmacol 2001;59:1094–9.
57. Ito Y, Pandey P, Place A, et al. The novel triterpenoid 2-cyano-3,12-dioxoolean-1,9-dien-28-oic acid induces apoptosis of human myeloid leukemia cells by a caspase-8-dependent mechanism. Cell Growth Differ 2000;11:261–7.

Combination of Vandetanib, Radiotherapy, and Irinotecan in the LoVo Human Colorectal Cancer Xenograft Model

Phyllis Wachsberger, PhD,* Randy Burd, PhD,† Anderson Ryan, PhD,‡ Constantine Daskalakis, PhD,§ and Adam P. Dicker, MD, PhD*

From the Departments of *Radiation Oncology and §Pharmacology and Experimental Therapeutics, Thomas Jefferson University, Philadelphia, PA; †Department of Nutritional Sciences, University of Arizona, Tucson, AZ; ‡AstraZeneca Pharmaceuticals, Alderley Park, Macclesfield, United Kingdom

*Reprinted from International Journal of Radiation Oncology*Biology*Physics, Volume 75, Edition 3, Wachsberger P, Burd R, Ryan A, Daskalakis C, Dicker AP: "Combination of Vandetanib, Radiotherapy, and Irinotecan in the LoVo Human Colorectal Cancer Xenograft Model", pages 843-853, November 1, 2009. Reprinted with Permission of Elseiver.*

Purpose: The tumor growth kinetics of the human LoVo colorectal xenograft model was assessed in response to vandetanib, an orally available receptor tyrosine kinase inhibitor, radiotherapy (RT), or irinotecan (CPT-11), as single therapies and in combination.

Methods and Materials: LoVo cells were injected subcutaneously into the right hind limb ($5x10^6$ cells in 100μL phosphate-buffered saline) of athymic NCR NUM mice and tumors were grown to a volume of 200–300mm^3 before treatment. Vandetanib was administered at 50 mg/kg daily orally for 14 days starting on Day 1. RT was given as three fractions (3x3 Gy) on Days 1, 2, and 3. CPT-11 was given at 15 mg/kg intraperitoneally on Days 1 and 3. Tumor volumes were measured on a daily basis and calculated by measuring tumor diameters with digital calipers in two orthogonal dimensions.

Results: All three single treatments (vandetanib, CPT-11, and radiation) significantly slowed LoVo colorectal tumor growth. Vandetanib significantly increased the antitumor effects of CPT-11 and radiation when given in combination with either of these treatments. These treatment combinations resulted in a slow tumor growth rate during the 2 weeks of vandetanib administration. The triple combination of vandetanib, CPT-11, and radiation produced the most marked improvement in response as observed by measurable shrinkage of tumors during the first week of treatment.

Conclusions: The tumor growth delay kinetics observed in this study of the LoVo colorectal model suggest concurrent and sustained post-sequencing of vandetanib with cytotoxic therapy may be beneficial in tumors of this type. ©2009 Elsevier Inc.

Key Words: Vandetanib, Radiotherapy, CPT-11, LoVo colorectal cancer, Angiogenesis inhibitor.

Introduction

Colorectal cancer (CRC) remains one of the leading causes of mortality worldwide. In recent years, the most widely used chemotherapy for metastatic CRC, fluoropyrimidine (5-fluorouracil [5-FU]) in combination with folinic acid, has been combined with newer, highly active cytotoxic agents. Among these agents is the DNA topoisomerase I inhibitor, irinotecan (CPT-11),[1] a potent DNA-targeting drug used in patients with CRC that is refractory to treatment with fluorouracil and leucovorin. This cytotoxic agent is, in turn, being combined with new molecular therapies targeting the tumor vasculature and key signaling pathways controlling tumor cell proliferation, angiogenesis, and survival in CRC. In this regard, the epidermal growth factor receptor (EGFR) plays an important role in CRC tumor growth and progression,[2] and cetuximab, a monoclonal antibody specific for EGFR, has been approved for use in combination with CPT-11 in patients with EGFR-expressing CRC refractory to CPT-11–based chemotherapy.[3] In addition, bevacizumab, a monoclonal antibody specific for vascular endothelial growth factor (VEGF-A), a key player in tumor angiogenesis in CRC as well as other solid tumors, has been approved for the treatment of metastatic CRC in combination with intravenous 5-FU–based chemotherapies.[4] Despite recent improvements in treatment for CRC, a need still remains to improve the performance of existing treatments and to establish the optimum scheduling and dosing of combined therapies.

Vandetanib (ZACTIMA) is an oral receptor tyrosine kinase inhibitor that, in recombinant enzyme assays, demonstrates potent activity against vascular endothelial growth factor receptor-2 (VEGFR-2) tyrosine kinase (the half maximal inhibitory concentration [IC_{50}]=40 nmol/L) with additional activity against EGFR (IC_{50}=500 nmol/L) and the rearranged during transfection (RET) tyrosine kinases (IC_{50}=130nM) tyrosine kinases.[5–8] Vandetanib has orphan-drug status in the United States and Europe for medullary thyroid cancer (in which RET activity is important) and is in Phase III development in non–small-cell lung cancer and medullary thyroid cancer. Phase II studies are ongoing to investigate its efficacy in other tumor types, thyroid cancer, hepatocellular carcinoma, and glioblastoma.

Vandetanib has been shown to enhance the efficacy of radiotherapy in subcutaneous and orthotopic tumor xenograft models.[9–13] The combination of vandetanib, radiation, and current chemotherapeutic agents used in CRC treatment has not been studied. Preclinical demonstration of efficacy of a combination protocol with novel agents plus radiation is usually considered crucial before clinical evaluation. The purpose of the present study was to examine the effect of vandetanib on the radiation response of a colorectal tumor model when administered in combination with CPT-11. It was hypothesized that simultaneous inhibition of VEGFR and EGFR by vandetanib in combination with the cytotoxic agent CPT-11 would interact to enhance radiation response and tumor control

in the human LoVo colorectal tumor cell model. The LoVo colorectal model expresses activated EGFR[14, 15] and is highly vascularized and therefore is an appropriate model to test the hypothesis.

Methods and Materials

Animal and tumor model

LoVo cell suspensions ($5x10^6$ cells in 100 µL phosphate buffered saline) were implanted subcutaneously into the right hind limbs of 6- to 8-week-old athymic NCR NUM mice (Taconic Farms, Hudson, NY). A subcutaneous xenograft model was chosen to facilitate radiation dosing and ease of tumor measurements. Tumors were allowed to grow for approximately 25 days, until reaching an approximate volume of 200–300mm^3 at the start of treatment (Day 1). All animals were randomized among treatment groups.

Drug treatment

Vandetanib (AstraZeneca, Macclesfield, UK) was administered by oral gavage at 50mg/kg daily for 14 days, starting on Day 1. Vandetanib dosing in this study was based on previous pharmacokinetic studies in mouse models predicting relevance of this dosing to clinical drug exposure in human patients.[16] CPT-11 was given at 15mg/kg intraperitoneally on Days 1 and 3.

Radiation treatment

Irradiation was performed on anesthetized mice using X-rays generated by a PanTak, 310 kVe X-ray machine, 0.25mm Cu+1mm Al added filtration, at 125cGy/min. Dosimetry was performed by an in-the-beam ionization chamber calibrated against a primary standard. Corrections were made daily for humidity, temperature, and barometric pressure. Mice were anesthetized with a combination of ketamine and acepromazine at a concentration of 37.5mg/kg and 0.2mg/kg, respectively, to provide 25–30 min of sedation. Each mouse was confined in a lead casing with its tumor-bearing leg extended through an opening on the side to allow the tumor to be irradiated locally. Radiation was administered as three daily fractions of 3 Gy each on Days 1, 2, and 3. On days when radiation was administered with vandetanib or CPT-1, vandetanib and CPT-11 were given approximately 2h before radiation, with vandetanib preceding CPT-11 administration.

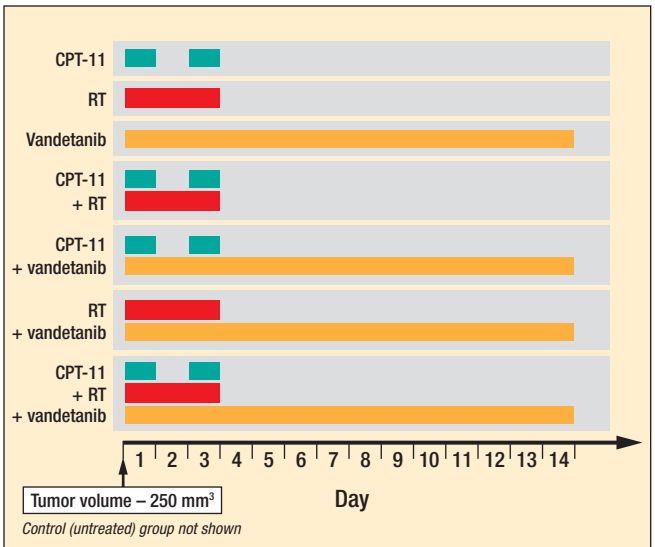

Figure 1. Summary of treatment groups. LoVo cells were implanted subcutaneously into the right hind limbs of athymic NCR NUM male mice. Mice were randomized into eight experimental groups (11–16 animals per group). Vandetanib was administered at 50 mg/kg daily orally for 14 days, starting on Day 1. CPT-11 was given at 15 mg/kg intraperitoneally on Days 1 and 3. Radiation was given as three fractions (3x3 Gy) on Days 1, 2, and 3.

Tumor measurement

Tumors were synchronized to be approximately 250 mm^3 at the start of treatment (Day 1) and were measured four to five times per week, for up to 6 weeks of follow-up, or until they reached 2,000 mm^3. Tumor size was determined by direct measurement with calipers and calculated by the formula: (smallest diameter^2 x widest diameter)/2. Tumors were not allowed to grow beyond 2,000 mm^3 in accordance with Institutional Animal Care and Use Committee regulations.

In vivo tumor necrosis

Tumors were collected from animals on Day 14 after the start of treatment for fixation and staining with hematoxylin and eosin. The area of necrosis was evaluated by image analysis and expressed as the percentage of the total tumor area.

Statistical analysis

Tumor growth was analyzed via mixed-effects regression, as previously described. The method was used because it does not depend on an arbitrary end point target tumor size, but uses the repeated tumor size measurements obtained over the entire study period, while appropriately handling unbalanced data (*i.e.*, different number of measurements for different animals) and the correlation of each animal's measurements over time. Mixed-effects regression yields generalizable parameters of interest (*e.g.*, average daily tumor growth rate, tumor doubling time), and can investigate treatment interactions and nonlinear patterns of tumor growth. The base-10 logarithm of tumor volume was modeled as a function of time and treatment. Linear or quadratic growth curves over time were fitted to the log-transformed data, depending on growth patterns in each treatment group. All statistical analyses were conducted in SAS 9.2 (SAS Institute Inc., Cary, NC, 1999–2001).

Results

The experiment involved three different treatments (vandetanib, CPT-11, and radiotherapy), as described above and summarized in Fig. 1. Data were collected from a total of 104 animals in eight experimental groups (11–16 animals per group) and are summarized in Fig. 2. Starting tumor sizes were comparable across groups, with geometric means ranging from 230 to 257mm^3 (p = 0.771). All treatments were well tolerated in the animals with no observable loss of body weight.

The three single-treatment groups (CPT-11, radiation, or vandetanib), as well as the combination of CPT-11 with radiation (Fig. 2) were fitted to log-transformed curves, whereas the three remaining groups that received combination treatments involving vandetanib showed a significantly nonlinear tumor growth and were fitted to quadratic curves.

Figure 3 shows the measured geometric mean tumor size graphically over time. Table 1 shows the corresponding calculated tumor growth parameters (daily tumor growth rate and tumor doubling time). Table 2 shows p values for group comparisons at 7, 14, and 21 days after start of treatment.

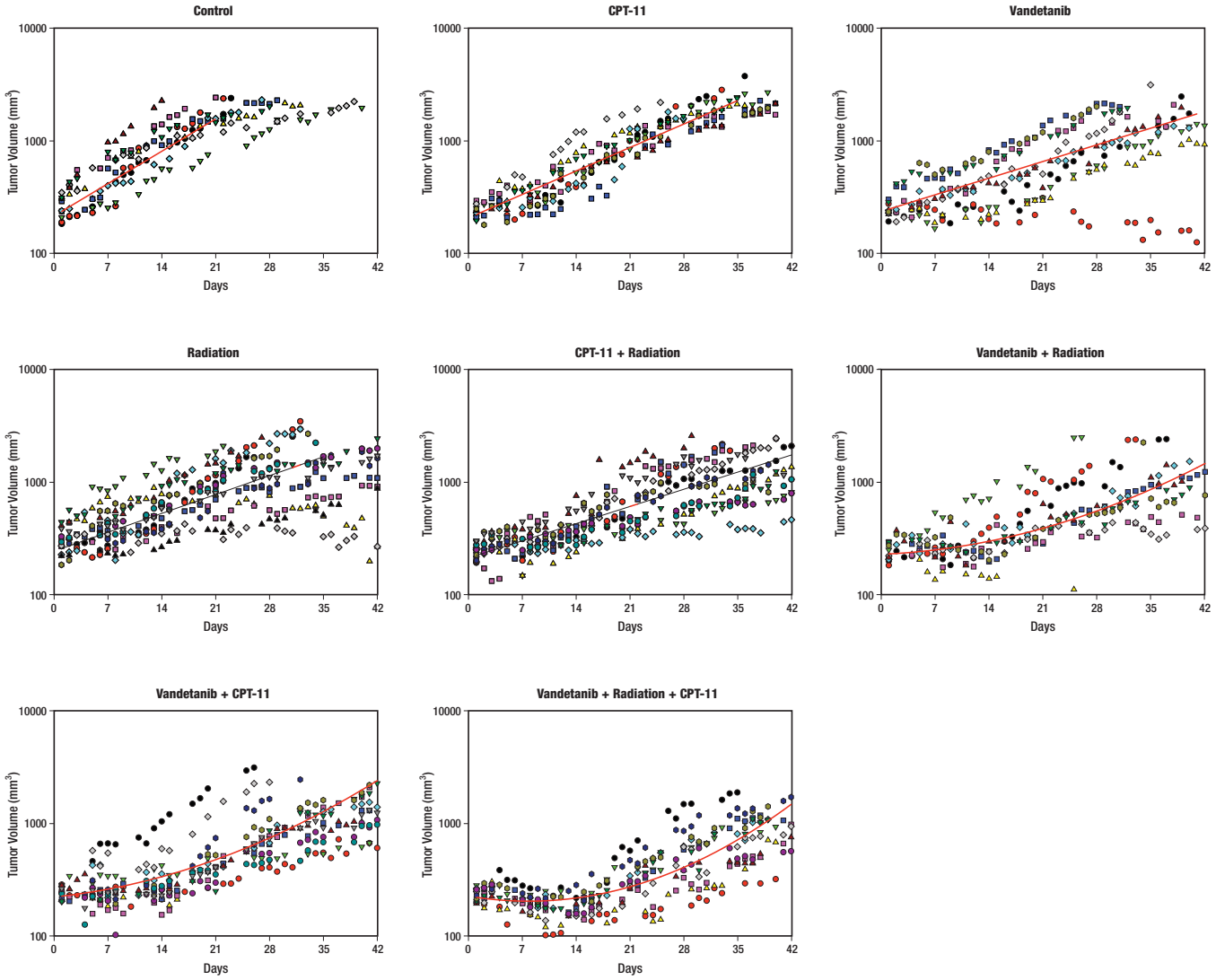

Figure 2. Tumor growth curves in LoVo xenografts treated with vandetanib, irinotecan (CPT-11), and/or radiation. Individual mouse data are shown for eight treatment groups (11–16 animals per group), along with fitted group curves. Vandetanib was administered at 50 mg/kg daily orally for 14 days, starting on Day 1. CPT-11 was given at 15 mg/kg intraperitoneally on Days 1 and 3. Radiation was given as three fractions (3x3 Gy) on Days 1, 2, and 3.

The control group had an estimated average daily tumor growth rate of 9.9%, corresponding to an average tumor doubling time of about 7 days (Table 1). All three single treatments resulted in a significant inhibition of tumor growth, compared with the control group (average daily tumor growth rates: CPT-11: 7.1%, $p = 0.015$; radiation: 5.6%, $p = 0.001$; vandetanib: 5.0%, $p = 0.001$). Vandetanib inhibited tumor growth significantly more than CPT-11 ($p = 0.043$), but not radiation ($p = 0.514$); radiation and CPT-11 were not significantly different ($p = 0.139$). The combination of CPT-11 with radiation produced a daily tumor growth rate of 5.1%, which was significantly lower than CPT-11 alone ($p = 0.015$) but comparable to radiation alone ($p = 0.560$). There was no significant (additive) interaction between CPT-11 and radiation ($p = 0.105$).

The remaining three groups that received treatment combinations involving vandetanib (with either CPT-11 or radiation, or with both CPT-11 and radiation), showed significant treatment interactions ($p = 0.001$ for the interaction between vandetanib and CPT-11 and between vandetanib and radiation) and nonlinear tumor growth patterns. Compared with single-treatment groups, growth was significantly delayed (and, in the triple-treatment combination, tumor volume actually decreased) early on, but progressively accelerated later, although it never exceeded that of the untreated controls (Fig. 3). Because of the nonlinearity of tumor growth in these groups, tumor growth parameters are not constant over time and comparisons depend on the time point referenced. Table 2 shows p values for Days 7, 14, and 21.

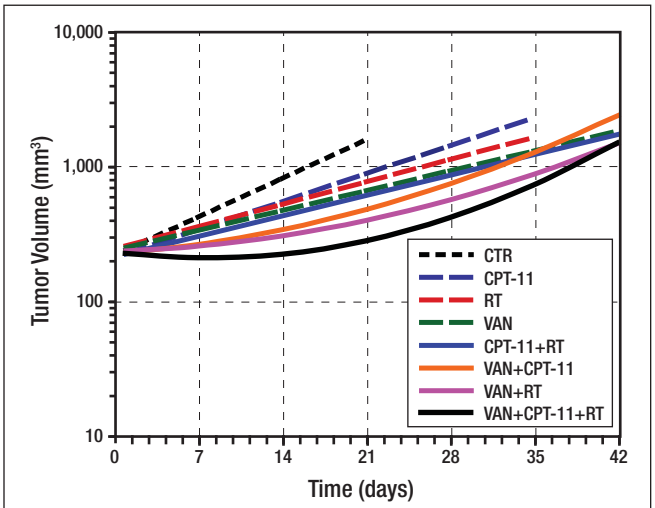

Figure 3. Estimated geometric mean tumor volume over time in LoVo xenografts treated with vandetanib, CPT-11, and/or radiation. Vandetanib was administered at 50 mg/kg daily orally for 14 days, starting on Day 1. CPT-11 was given at 15 mg/kg intraperitoneally on Days 1 and 3. Radiation was given as three fractions (3x3 Gy) on Days 1, 2, and 3.

During the first week of treatment, animals receiving the combination of vandetanib with CPT-11 had average daily tumor growth rate of less than 3.5%, significantly lower than CPT-11 alone and marginally so compared with vandetanib alone (p = 0.001 and 0.058, respectively, after 7 days). By the end of the 2-week vandetanib treatment, the tumor growth rate in the combination group (4.6%) was still significantly lower than for CPT-11 alone (p = 0.015) but comparable to that for vandetanib alone (p = 0.682). By the third and fourth weeks, tumor growth had reached levels similar to those seen in the single-treatment groups (Fig. 3, Table 1).

The combination of vandetanib with radiation resulted in a similar pattern of nonlinear tumor growth inhibition. After the first 7 days, the average daily tumor growth rate of 2.1% was significantly lower than for either radiation alone or vandetanib alone (p = 0.005 and 0.019, respectively). After 14 days, the tumor growth rate in the combination group had accelerated to 3.4% and was only marginally lower than for radiation alone and comparable to that for vandetanib alone (p=0.080 and 0.212, respectively). By the third and fourth weeks, tumor growth had become similar to that seen in the single-treatment groups (Fig. 3, Table 1).

Despite delaying tumor growth in the initial weeks, the treatment combinations induced only modest levels of tumor necrosis (10–20%), with no significant differences between treatment groups (Fig. 4).

The pattern of tumor growth in the group that received the triple-treatment combination reflected both the interaction between vandetanib and CPT-11 and that between vandetanib and radiation (as mentioned previously). Thus, during the first week, instead of the delayed tumor growth seen in the two-treatment combinations, tumor volume in the triple-treatment combination actually decreased (p = 0.001 vs. vandetanib plus CPT-11, and 0.052 vs. vandetanib plus radiation). After that time, similar to the two-treatment combinations that involved vandetanib, tumor growth started accelerating. By the end of the third week, tumor growth in the triple-treatment combination group was similar to that in the two-treatment combination groups involving vandetanib, and by the fourth week, it was similar to that in the single-treatment groups.

Discussion

Relatively little is known about the antitumor effects of combining cytotoxic drugs, radiotherapy, and novel targeted therapies that specifically interfere with signaling pathways controlling cancer proliferation, angiogenesis, and survival. In the present study, vandetanib, a potent inhibitor of both VEGFR and EGFR signaling, was combined with CPT-11 or radiation, to determine if greater anti-colorectal tumor activity can be obtained.

This study demonstrated that all three single treatments (vandetanib, CPT-11, and radiation) significantly slowed LoVo colorectal tumor growth. Previous studies with single-agent vandetanib demonstrated that chronic oral administration reduced tumor vascularity and tumor growth in a variety of xenograft models, including CRC.[7, 17] In the clinic, the safety and tolerability of vandetanib has been demonstrated in patients with advanced colorectal cancer as well as other solid tumors.[18]

Table 1. Estimates of the average daily tumor growth rate and average tumor doubling time, by treatment group

	Time (days) †					
	1	7	14	21	28	35
	%Δ(T_{2x})	%Δ(T_{2x})	%Δ(T_{2x})	%Δ(T_{2x})	%Δ(T_{2x})	%Δ(T_{2x})
CTR	9.9 (7.4)					
CPT-11	7.1 (10.2)					
RT	5.6 (12.7)					
VAN	5.0 (14.3)					
CPT-11 + RT	5.1 (13.9)					
VAN + CPT-11	1.9 (37.1)	3.2 (22.2)	4.6 (15.5)	6.0 (11.9)	7.4 (9.7)	8.9 (8.2)
VAN + RT	0.9 (75.4)	2.1 (33.4)	3.4 (20.9)	4.7 (15.2)	6.0 (11.9)	7.3 (9.8)
VAN + CPT-11 + RT	-2.1 N/A	0.0 N/A	2.4 (28.7)	4.9 (14.5)	7.4 (9.7)	9.9 (7.3)

%Δ: estimated average daily rate of increase/decrease of tumor volume (%).
T2x: estimated average doubling time of tumor volume (in days).
N/A: not applicable (tumor shrinks or is stable).
CTR, CPT-11, RT, VAN, and CPT-11+VAN groups had log-linear tumor growth, so their parameters were constant over time. The remaining groups did not have log-linear tumor growth, so their parameters were changing over time.

Table 2. P-values for comparisons of treatment groups, on days 7, 14, and 21, after the start of treatment

	Day 7	Day 14	Day 21
CTR			
CPT-11		0.015 vs. CTR; 0.139 vs. RT; 0.043 vs. VAN	
RT		0.001 vs. CTR; 0.139 vs. CPT-11; 0.514 vs. VAN	
VAN		0.001 vs. CTR; 0.043 vs. CPT-11; 0.514 vs. RT	
CPT-11 + RT		0.001 vs. CPT-11; 0.560 vs. RT	
VAN + CPT-11	0.001 vs. CPT-11; 0.058 vs. VAN	0.015 vs. CPT-11; 0.682 vs. VAN	0.346 vs. CPT-11; 0.395 vs. VAN
VAN + RT	0.005 vs. RT; 0.019 vs. VAN	0.080 vs. RT; 0.212 vs. VAN	0.496 vs. RT; 0.830 vs. VAN
VAN + CPT-11 + RT	0.001 vs. CPT-11; 0.001 vs. RT; 0.001 vs. VAN 0.001 vs. CPT-11+RT; 0.001 vs. VAN+CPT-11; 0.052 vs. VAN+RT	0.001 vs. CPT-11; 0.001 vs. RT; 0.007 vs. VAN 0.001 vs. CPT-11+RT; 0.017 vs. VAN+CPT-11; 0.407 vs. VAN+RT	0.011 vs. CPT-11; 0.366 vs. RT; 0.917 vs. VAN 0.766 vs. CPT-11+RT; 0.294 vs. VAN+CPT-11; 0.868 vs. VAN+RT

CTR, CPT-11, RT, VAN, and CPT-11+VAN groups had log-linear tumor growth and therefore comparisons do not depend on time.
The remaining groups did not have log-linear tumor growth and therefore comparisons that involve them depend on time.

Vandetanib induced manageable normal tissue toxicities related to inhibition of EGFR and VEGFR signaling such as diarrhea, rash, and hypertension.[19, 20] The effect of combining radiation and vandetanib on normal tissue is currently unknown, however it has been shown in both preclinical and clinical trials that use of VEGF inhibitors with radiation may result in higher rates of normal tissue toxicity such as induction of thrombosis, hemorrhage, and bowel toxicities.[21–23] In contrast, it was postulated that combination of radiotherapy with inhibitors of angiogenesis may actually decrease these risks because radiotherapy has been used to prevent hemorrhage.[24] Overall, the investigation of agents such as vandetanib in combination with radiation in normal tissue is lacking, and thus will be a major focus in the future.

As previously discussed, single-agent vandetanib has dual tyrosine kinase inhibitory activity against VEGFR-2 and EGFR, which allows it to target two key pathways responsible for tumor growth (*i.e.*, tumor angiogenic signaling, tumor cell proliferation). It has been speculated that dual suppression may be critical for sustained suppression of tumor growth, especially because the EGFR and VEGFR pathways are linked and exhibit cross-talk.[25] In addition, vandetanib can also enhance the antiproliferative activity of selective EGFR inhibitors such as cetuximab, thereby potentiating suppression of EGFR signaling.[17]

The present study confirmed that vandetanib, chronically administered over 2 weeks, slowed tumor growth in a colorectal tumor model, and, under the dosing conditions of this study, slowed tumor growth to a greater extent than CPT-11 alone and to a similar level to radiation alone. Moreover, vandetanib significantly increased the antitumor effects of CPT-11 and radiation, when given in combination with either of these treatments. In particular, these treatment combinations resulted in a slow tumor growth rate during the 2 weeks of vandetanib administration. These results confirm an earlier study by Troiani *et al.*,[26] in which vandetanib

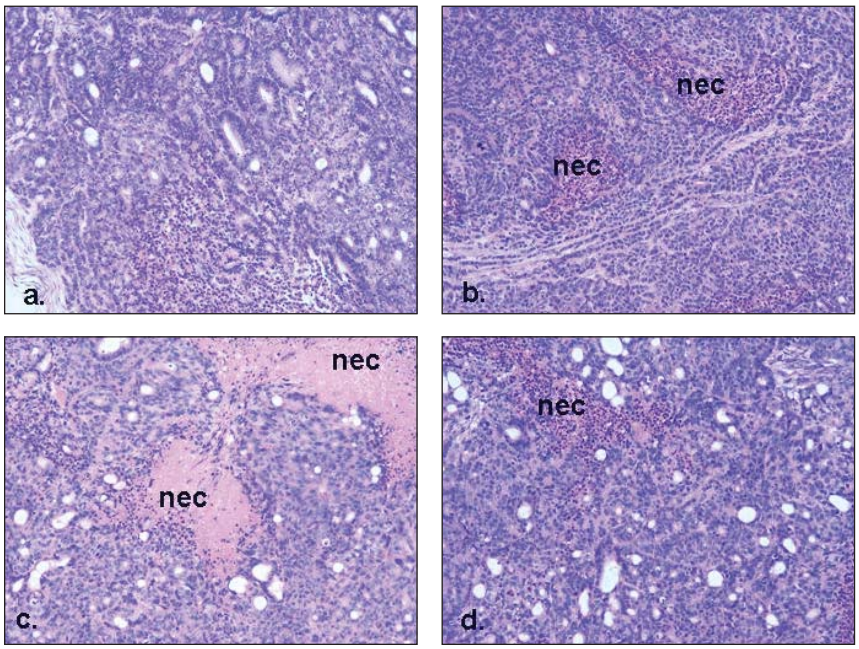

Figure 4. Hematoxylin and eosin stained sections of LoVo colorectal xenografts. All tumors were collected from animals on Day 14 after the start of treatment. Areas of necrosis are denoted by nec. Magnification 20x. **(a)** Control (untreated) tumor, showing 2% necrosis. **(b)** Tumor from animal after administration of last dose of vandetanib, showing 15% necrosis. **(c)** Tumor from animal after administration of CPT-11 and RT, showing 20% necrosis. **(d)** Tumor from animal after administration of vandetanib and CPT-11, showing 10% necrosis.

(25mg/kg/day) administered in combination with CPT-11 exhibited high antitumor activity in HT29-tumor–bearing nude mice. Troiani *et al.* showed a correlation between this dosing schedule and enhanced EGFR and VEGFR signal inhibition.

In the present study, the triple combination of vandetanib, CPT-11, and radiation produced the most marked improvement in response in the LoVo- tumor–bearing mice. The triple treatment produced a measurable shrinkage of tumors during the first week of treatment. The combination of vandetanib, chemotherapy (gemcitabine), and radiation has also been previously shown to significantly inhibit tumor progression in a pancreatic tumor model.[27] Importantly, the present study also investigated the kinetics of tumor growth, both during and after a course of treatment. It was demonstrated that the addition of vandetanib significantly enhanced the initial antitumor effect of chemo-radiation. However, when vandetanib treatment ended, tumor growth returned to near control (untreated) levels. Therefore, these data support the rationale of adding an antivascular agent to cytotoxic therapies and provide valuable information for the design of therapeutic protocols.

The precise mechanisms leading to initial tumor regression with the combined therapies in this study are not known. Analysis of interactions between cytotoxic agents and vandetanib is complex, given that both the tumor cells and the tumor microenvironment are affected. In this connection, radiation can kill not only tumor cells but also endothelial cells of the tumor vasculature, thereby affecting the radiosensitivity of the tumor (28, 29). In addition, cytotoxic agents have mechanisms of cell killing that are different from the targeted agent. Both radiation and CPT-11 kill cells through DNA damage. Both chemotherapy and radiation can also alter cellular signaling pathways by inducing EGFR phosphorylation and through the growth factor signaling pathway, contribute to tumor cell proliferation and survival.[30–32] Preclinical studies have also shown that cytotoxic therapy alone, such as radiation, can result in intensification of angiogenic processes.[33] After cytotoxic treatment, upregulation of vascular growth factors and their receptors occurs, which contributes to tumor recurrence and progression.[34] Direct upregulation of VEGF after irradiation of various cancer cell lines has been reported.[35] Radiation also induces transient tumor hypoxia which results in upregulation of hypoxia inducible factor-1 (HIF-1) which can stimulate VEGF and VEGFR-2 expression. Therefore, simultaneous inhibition of both VEGFR and EGFR signaling through chronic administration of vandetanib in combination with cytotoxic therapy is expected to suppress the upsurge in pro-proliferative and angiogenic signaling resulting from CPT-11 and radiation-induced EGFR and VEGF. This suppression will thereby lead to inhibition of vascular protective mechanisms and growth factor mechanisms contributing to tumor regrowth.

The increased tumor growth that was seen in this study after discontinuation of vandetanib suggests that inhibition of angiogenic and pro-proliferative signaling is readily reversed. The current observations are in agreement with a number of both preclinical and clinical studies showing that tumors can adapt to anti-angiogenic treatment by undergoing "evasive resistance" to angiogenesis inhibitors.[36] Mechanisms of resistance include upregulation of alternative proangiogenic signaling pathways as well as recruitment of bone marrow–derived proangiogenic cells.[37, 38] In addition, administration of vandetanib itself has been observed to increase VEGF production in certain cancer cell lines as well as in tumor xenografts,[39, 40] thereby suggesting an additional contributing mechanism to tumor relapse. More studies will be needed to determine whether additional angiogenic pathways may be induced by triple modality treatment.

Conclusions

The results of this study provide a scientific rationale for testing the combination of vandetanib, CPT-11, and radiation in patients with CRC. Although the best schedule and sequencing for this triple modality treatment has yet to be determined, the tumor growth delay kinetics observed in this study suggest that improvement in colorectal tumor response can be obtained by concurrent and sustained post-sequencing of vandetanib with cytotoxic therapy, keeping in mind that prolonged chronic administration of the receptor tyrosine kinase inhibitors may lead to the development of resistance and the requirement for additional therapeutic agents as seen with other targeted agents, such as imatinib and gefitinib.[41, 42]

References

1. Tewes M, Schleucher N, Achterrath W, *et al.* Capecitabine and irinotecan as first-line chemotherapy in patients with metastatic colorectal cancer: Results of an extended phase I study. *Ann Oncol* 2003;14:1442–1448.
2. Roberts RB, Min L, Washington MK, *et al.* Importance of epidermal growth factor receptor signaling in establishment of adenomas and maintenance of carcinomas during intestinal tumorigenesis. *Proc Natl Acad Sci U S A* 2002;99:1521–1526.
3. Cunningham D, Humblet Y, Siena S, *et al.* Cetuximab monotherapy and cetuximab plus irinotecan in irinotecan-refractory metastatic colorectal cancer. *N Engl J Med* 2004;351:337–345.
4. Hurwitz H, Fehrenbacher L, Novotny W, *et al.* Bevacizumab plus irinotecan, fluorouracil, and leucovorin for metastatic colorectal cancer. *N Engl J Med* 2004;350:2335–2342.
5. Carlomagno F, Vitagliano D, Guida T, *et al.* ZD6474, an orally available inhibitor of KDR tyrosine kinase activity, efficiently blocks oncogenic RET kinases. *Cancer Res* 2002;62:7284–7290.
6. Ciardiello F, Caputo R, Damiano V, *et al.* Antitumor effects of ZD6474, a small molecule vascular endothelial growth factor receptor tyrosine kinase inhibitor, with additional activity against epidermal growth factor receptor tyrosine kinase. *Clin Cancer Res* 2003;9:1546–1556.
7. Ryan AJ, Wedge SR. ZD6474 – a novel inhibitor of VEGFR and EGFR tyrosine kinase activity. *Br J Cancer* 2005;92(Suppl1):S6–S13.
8. Wedge SR, Ogilvie DJ, Dukes M, *et al.* ZD6474 inhibits vascular endothelial growth factor signaling, angiogenesis, and tumor growth following oral administration. *Cancer Res* 2002;62:4645–4655.
9. Brazelle WD, Shi W, Siemann DW. VEGF-associated tyrosine kinase inhibition increases the tumor response to single and fractionated dose radiotherapy. *Int J Radiat Oncol Biol Phys* 2006;65:836–841.
10. Damiano V, Melisi D, Bianco C, *et al.* Cooperative antitumor effect of multitargeted kinase inhibitor ZD6474 and ionizing radiation in glioblastoma. *Clin Cancer Res* 2005;11:5639–5644.
11. Frederick B, Gustafson D, Bianco C, *et al.* ZD6474, an inhibitor of VEGFR and EGFR tyrosine kinase activity in combination with radiotherapy. *Int J Radiat Oncol Biol Phys* 2006;64:33–37.
12. Sandstrom M, Johansson M, Bergstrom P, *et al.* Effects of the VEGFR inhibitor ZD6474 in combination with radiotherapy and temozolomide in an orthotopic glioma model. *J Neurooncol* 2008;88:1–9.
13. Williams KJ, Telfer BA, Brave S, *et al.* ZD6474, a potent inhibitor of vascular endothelial growth factor signaling, combined with radiotherapy: Schedule-dependent enhancement of antitumo activity. *Clin Cancer Res* 2004;10:8587–8593.
14. Koizumi F, Kanzawa F, Ueda Y, *et al.* Synergistic interaction between the EGFR tyrosine kinase inhibitor gefitinib ("Iressa") and the DNA topoisomerase I inhibitor CPT-11 (irinotecan) in human colorectal cancer cells. *Int J Cancer* 2004;108:464–472.
15. Nyati MK, Maheshwari D, Hanasoge S, *et al.* Radiosensitization by pan ErbB inhibitor CI-1033 in vitro and in vivo. *Clin Cancer Res* 2004;10:691–700.
16. Gustafson DL, Bradshaw-Pierce EL, Merz AL, *et al.* Tissue distribution and metabolism of the tyrosine kinase inhibitor ZD6474 (Zactima) in tumor-bearing nude mice following oral dosing. *J Pharmacol Exp Ther* 2006;318:872–880.
17. Morelli MP, Cascone T, Troiani T, *et al.* Anti-tumor activity of the combination of cetuximab, an anti-EGFR blocking monoclonal antibody and ZD6474, an inhibitor of VEGFR and EGFR tyrosine kinases. *J Cell Physiol* 2006;208:344–353.
18. Morabito A, Piccirillo MC, Falasconi F, *et al.* Vandetanib (ZD6474), a dual inhibitor of vascular endothelial growth factor receptor (VEGFR) and epidermal growth factor receptor (EGFR) tyrosine kinases: Current status and future directions. *Oncologist* 2009;14:378–390.
19. Michael M, Gibbs P, Smith R, *et al.* Open-label phase I trial of vandetanib in combination with mFOLFOX6 in patients with advanced colorectal cancer. *Invest New Drugs* 2009;27:253–261.
20. Natale RB, Bodkin D, Govindan R, *et al.* Vandetanib versus gefitinib in patients with advanced non-small-cell lung cancer: Results from a two-part, double-blind, randomized Phase II Study. *J Clin Oncol* 2009;27:2523–2529.
21. Johnson DH, Fehrenbacher L, Novotny WF, *et al.* Randomized phase II trial comparing bevacizumab plus carboplatin and paclitaxel with carboplatin and paclitaxel alone in previously untreated locally advanced or metastatic non-small-cell lung cancer. *J Clin Oncol* 2004;22:2184–2191.

22. Levine RJ, Maynard SE, Qian C, *et al.* Circulating angiogenic factors and the risk of preeclampsia. *N Engl J Med* 2004;350:672–683.
23. Senan S, Smit EF. Design of clinical trials of radiation combined with antiangiogenic therapy. *Oncologist* 2007;12:465–477.
24. Shibuya K, Komaki R, Shintani T, *et al.* Targeted therapy against VEGFR and EGFR with ZD6474 enhances the therapeutic efficacy of irradiation in an orthotopic model of human non-small-cell lung cancer. *Int J Radiat Oncol Biol Phys* 2007;69:1534–1543.
25. Pennell NA, Lynch TJ Jr,. Combined inhibition of the VEGFR and EGFR signaling pathways in the treatment of NSCLC. *Oncologist* 2009;14:399–411.
26. Troiani T, Serkova NJ, Gustafson DL, *et al.* Investigation of two dosing schedules of vandetanib (ZD6474), an inhibitor of vascular endothelial growth factor receptor and epidermal growth factor receptor signaling, in combination with irinotecan in a human colon cancer xenograft model. *Clin Cancer Res* 2007;13:6450–6458.
27. Bianco C, Giovannetti E, Ciardiello F, *et al.* Synergistic antitumor activity of ZD6474, an inhibitor of vascular endothelial growth factor receptor and epidermal growth factor receptor signaling, with gemcitabine and ionizing radiation against pancreatic cancer. *Clin Cancer Res* 2006;12:7099–7107.
28. Garcia-Barros M, Paris F, Cordon-Cardo C, *et al.* Tumor response to radiotherapy regulated by endothelial cell apoptosis. *Science* 2003;300:1155–1159.
29. Paris F, Fuks Z, Kang A, *et al.* Endothelial apoptosis as the primary lesion initiating intestinal radiation damage in mice. *Science* 2001;293:293–297.
30. Balaban N, Moni J, Shannon M, *et al.* The effect of ionizing radiation on signal transduction: Antibodies to EGF receptor sensitize A431 cells to radiation. *Biochim Biophys Acta* 1996;1314:147–156.
31. Schmidt-Ullrich RK, Mikkelsen RB, Dent P, *et al.* Radiation-induced proliferation of the human A431 squamous carcinoma cells is dependent on EGFR tyrosine phosphorylation. *Oncogene* 1997;15:1191–1197.
32. Van SS, Kyula J, Kelly DM, *et al.* Chemotherapy-induced epidermal growth factor receptor activation determines response to combined gefitinib/chemotherapy treatment in non-small cell lung cancer cells. *Mol Cancer Ther* 2006;5:1154–1165.
33. Koukourakis MI, Giatromanolaki A, Sivridis E, *et al.* Squamous cell head and neck cancer: Evidence of angiogenic regeneration during radiotherapy. *Anticancer Res* 2001;21:4301–4309.
34. Taylor AP, Osorio L, Craig R, *et al.* Tumor-specific regulation of angiogenic growth factors and their receptors during recovery from cytotoxic therapy. *Clin Cancer Res* 2002;8:1213–1222.
35. Gorski DH, Beckett MA, Jaskowiak NT, *et al.* Blockage of the vascular endothelial growth factor stress response increases the antitumor effects of ionizing radiation. *Cancer Res* 1999;59:3374–3378.
36. Bergers G, Hanahan D. Modes of resistance to anti-angiogenic therapy. *Nat Rev Cancer* 2008;8:592–603.
37. Casanovas O, Hicklin DJ, Bergers G, *et al.* Drug resistance by evasion of antiangiogenic targeting of VEGF signaling in latestage pancreatic islet tumors. *Cancer Cell* 2005;8:299–309.
38. Du R, Lu KV, Petritsch C, *et al.* HIF1alpha induces the recruitment of bone marrow-derived vascular modulatory cells to regulate tumor angiogenesis and invasion. *Cancer Cell* 2008;13:206–220.
39. Sasaki T, Tanno S, Shibukawa K, *et al.* Administration of VEGF receptor tyrosine kinase inhibitor increases VEGF production causing angiogenesis in human small-cell lung cancer xenografts. *Int J Oncol* 2008;33:525–532.
40. Showalter TN, Daroczi B, Halko R, *et al.* ZD6474 enhances radiation therapy in human glioblastoma xenografts which contain the EGFRvIII mutation or overexpress wtEGFR. *Abstract, Radiation Research Society Annual Meeting 2008 (Boston, MA)* Radiation Research Society Annual Meeting 2008.
41. Komarova NL, Katouli AA, Wodarz D. Combination of two but not three current targeted drugs can improve therapy of chronic myeloid leukemia. *PLoS ONE* 2009;4:e4423.
42. Okabe T, Okamoto I, Tsukioka S, *et al.* Addition of S-1 to the epidermal growth factor receptor inhibitor gefitinib overcomes gefitinib resistance in non-small cell lung cancer cell lines with MET amplification. *Clin Cancer Res* 2009;15:907–913.

Does Intraoperative Radiation Therapy Improve Local Tumor Control in Patients Undergoing Pancreaticoduodenectomy for Pancreatic Adenocarcinoma? A Propensity Score Analysis

Timothy N. Showalter,[1] Atul S. Rao,[3] P. Rani Anné,[1] Francis E. Rosato,[3] Ernest L. Rosato,[3] Jocelyn Andrel,[2] Terry Hyslop,[2] Xia Xu,[1] Adam C. Berger[3]

[1]Department of Radiation Oncology, [2]Division of Biostatistics, and [3]Department of Surgery Thomas Jefferson University, Philadelphia, PA

Annals of Surgical Oncology, Volume 16, Edition 8, August, 2009, pages 2116-22, "Does intraoperative radiation therapy improve local tumor control in patients undergoing pancreaticoduodenectomy for pancreatic adenocarcinoma? A propensity score analysis". Authors: Showalter TN, Rao AS, Anné PR, Rosato FE, Rosato EL, Andrel J, Hyslop T, Xu X, Berger AC. Reprinted with kind permission of Springer Science and Business Media.

Abstract

Background: Locoregional recurrence (LRR) is an important factor after pancreaticoduodenectomy (PD) for pancreatic cancer. IORT administered to the resection bed may improve local tumor control.

Methods: We performed a retrospective analysis of patients who underwent PD at Thomas Jefferson University Hospital (TJUH) between 1995 and 2005 to identify patients who underwent resection with and without intraoperative radiation therapy (IORT). Data collected included age, gender, complications, margin status, stage, survival, and recurrence. Unadjusted analyses of the IORT and non-IORT groups were performed using Fisher's chi-square method for discrete variables and Wilcoxon Rank Sum test for continuous variables. To account for biases in patient selection for IORT, a propensity score was calculated for each patient and adjusted statistical analyses were performed for survival and recurrence outcomes.

Results: Between January 1995 and November 2005, 122 patients underwent PD for perimpullary tumors, including 99 pancreatic cancers. Of this group, 37 patients were treated with IORT, and there was adequate follow-up information for a group of 46 patients who underwent PD without IORT. The IORT group contained a higher percentage of Stage IIB or higher tumors (65%) than in the non-IORT group (39.1%), though differences in stage did not reach significance ($p = 0.16$). There was a non-significant decrease in the rate of LRR in patients who had IORT (39% non-IORT vs. 23% IORT, $p = 0.19$). The median survival time of patients who received IORT was 19.2 months, which was not significantly different than patients managed without IORT, 21.0 months (p=0.78). In the propensity analyses, IORT did not significantly influence survival or recurrence after PD.

Conclusions: IORT can be safely added to management approaches for resectable pancreatic cancer, with acceptable morbidity and mortality. IORT did not improve loco-regional control and did not alter survival for patients with resected pancreatic cancer. IORT is an optional component of adjuvant chemoradiation for pancreatic cancer. In the future, IORT may be combined with novel therapeutic agents in the setting of a clinical trial in order to attempt to improve outcomes for patients with pancreatic cancer.

Surgical resection is an essential component in the therapeutic approach to patients with localized pancreatic cancer. Despite refinements in surgical technique, local and distant recurrences are common. Long-term survival rates are low for patients with resectable tumors, with 15-20% 5-year survival reported among patients who undergo pancreaticoduodenectomy (PD) alone.[1,2] In a review of resection margins of 72 patients who underwent PD, Willett *et al.* detected a positive margin in 51% of cases; this factor was associated with inferior survival and local control when compared with those patients with negative surgical margins.[2] Although there is controversy regarding the appropriate components of adjuvant management of resected pancreatic cancer,[3-7] outcomes achieved after surgery alone continue to be poor; therefore, the need remains for adjuvant therapy to improve local control and survival.[3-8] In the United States, adjuvant chemoradiotherapy (CRT) is performed as part of the standard therapeutic paradigm, based on the recurrence patterns of pancreatic cancer after surgery.[8,9]

Intraoperative radiation therapy (IORT), the delivery of a single, large dose of irradiation at the time of surgery, was developed in order to administer higher doses of irradiation while displacing or shielding adjacent normal tissue structures from radiation exposure.[10] In pancreatic cancer, IORT has been offered for unresectable tumors to provide local tumor control and palliation of pain,[11-16] and for resectable tumors in an effort to improve local control and survival after PD.[11-19] Although a definitive survival benefit has not been observed, improvement of local control by IORT at the time of PD for resectable pancreatic cancer is supported by retrospective data, as well as by a prospective, randomized trial conducted at the National Cancer Institute (NCI).[19-21]

At our institution, IORT has been offered since 1986 in a dedicated operating suite located in the radiotherapy department for patients with either resectable or unresectable pancreatic cancer. IORT was considered for all patients undergoing PD at our institution until 1998. Since then, IORT has been reserved for patients with larger tumors with higher risk of positive margins, as visualized by the surgeon on preoperative imaging. Prior reports from our institution have described outcomes of patients who received IORT for resectable and unresectable pancreatic cancer prior to 1995.[13, 22] The current study evaluates outcomes for patients who received treatment for resectable pancreatic cancer from 1995 to 2005. As a result of physician bias for the use of IORT in more advanced-stage pancreatic cancer at our institution, it was not possible to identify a comparative group of patients for use in a matched pair analysis. Therefore, in order to account for the biases inherent in the nonrandom treatment assignment for patients in the current study, analyses of survival and recurrence were adjusted using propensity scoring.[23] In this way, we attempted to minimize the influence of confounding patient- and tumor-related variables in order to assess the contribution of IORT to local tumor control and survival of patients with localized, resectable pancreatic cancer treated at our institution.

Materials & Methods

A prospective tumor registry database was searched to identify all patients who underwent PD at Thomas Jefferson University during 1995-2005. The study was performed with approval of the institutional review board at Thomas Jefferson University. These patients were further divided into those who did and did not receive IORT. We collected data regarding age, gender, margin status, stage, survival and recurrence. Loco-regional recurrence (LRR) was defined as recurrence within the tumor bed or regional lymph nodes. Systemic recurrence (SR) consisted of recurrence in the liver, peritoneum, lungs, bone, or other distant site. Overall survival (OS) and time to LRR were measured from the date of surgery. Given the institutional bias towards IORT for larger tumors during much of the study period, a difference between treatment groups was anticipated in the statistical analysis. A propensity score, a statistical method to adjust for nonrandom treatment decisions in observational studies, was also calculated for each patient using a logistic regression model.[23]

Treatment Policy

All patients were treated according to institutional treatment policies during 1995-2005. As a general rule, IORT was considered for all patients prior to 1998 and subsequently for patients with larger tumors based on review of preoperative imaging by the attending surgeon. For these patients, surgery was performed in an operating room located in the radiation oncology department, an arrangement selected to facilitate IORT delivery. IORT was delivered using 6-15 MeV electrons and cone sizes selected in order to deliver a dose of 10-20 Gy to a field encompassing the pancreatic tumor bed within the 90% isodose line. Regional lymph nodes were not included in the target volume for most cases. The cone size, treatment set-up, and immobilization were selected in order to treat the target volume while minimizing exposure of adjacent normal tissue structures. The standard dose, 15 Gy, was reduced to 10 Gy for either large treatment volumes or margins that were clearly negative. For larger tumors, 20 Gy was often prescribed. In cases where adjuvant external beam radiation therapy (RT) was also delivered, a dose of 45-50.4 Gy was prescribed using a conformal, four-field radiation technique.

Statistical Analysis

Simple descriptive statistics were generated, and unadjusted associations with IORT were determined using Fisher's Chi Square test for categorical variables and using the Wilcoxon rank sum test for continuous variables. The propensity score, which was calculated for all patients included in the analysis using a logistic regression model, included resection status, AJCC Stage, differentiation, age, race, and sex. Propensity scores were incorporated as a categorical variable in the statistical analyses based on quartiles. The association of IORT with the primary outcome of survival was determined using a Cox proportional hazards model. The Cox proportional hazards model included IORT, the propensity score (by quartile), adjuvant chemotherapy, and adjuvant radiotherapy. Association of IORT with the secondary outcomes of any recurrence, loco-regional recurrence, and systemic recurrence was determined using logistic regression models. Included in the logistic regression models for adjusted analyses of recurrence were IORT, the propensity score (by quartile), adjuvant chemotherapy, and adjuvant radiotherapy.

Results

From January 1995 to November 2005, 122 patients underwent PD for periampullary tumors, including 99 pancreatic cancers. We identified 37 patients with pancreatic cancer who were treated with IORT. Among the remaining 62 patients with pancreatic cancer treated without IORT, adequate follow-up data could be obtained for 46 patients, who comprised the non-IORT group used in the statistical analyses. The median patient age in the IORT group was 64 years (inter-quartile range, 55-70 years); in the non-IORT group, the median age was 67 years (inter-quartile range, 59-74 years). The IORT group demonstrated non-significant trends toward more advanced stage tumors (p=0.16) and a higher rate of positive margins (p=0.26). A higher proportion of patients received adjuvant chemotherapy after PD with IORT than after PD alone (p=0.05) (Table 1). There were 2 perioperative deaths in the IORT group (5.4%) and none in the non-IORT group (p=0.20). Rates of perioperative complications were similar, 46% in the IORT group versus 40% in the non-IORT group. The median follow-up among surviving patients was 21 months.

Recurrence and Survival

Recurrence data were available for 80% of all patients, including 30 IORT patients (81%) and 36 non-IORT patients (78%). Rates of loco-regional recurrence (LRR) (Figure 1) or any recurrence (Figure 2) were not significantly different between the IORT and non-IORT groups. Among non-IORT patients, there was loco-regional recurrence (LRR) in 39%, systemic recurrence (SR) in 50%, and any recurrence in 69%. In the IORT group, LRR in 23%, SR in 57% of patients, with, and recurrence was observed in 67% (Table 2). Liver metastases were the most common form of SR. LRR in the absence of SR was observed in 2 patients (7%) in the IORT group and in 7 patients in the non-IORT group (19%). LRR was not significantly different between the IORT and non-IORT groups (p=0.20). The median survival time of patients undergoing IORT was 19.2 months, which was not significantly different than patients managed without IORT, 21.0 months (p=0.49) (Figure 3).

Propensity Score Analysis

In the adjusted, propensity score analysis of the association of IORT with survival, IORT was not associated with significant improvement of survival time (Table 3). The Cox regression model for survival included IORT status with propensity score (by quartile), as well as adjuvant RT and chemotherapy. The propensity score-adjusted analyses of the association

Table 1. Tumor- and treatment-related characteristics for 37 IORT patients and 46 non-IORT patients with resected pancreatic cancer.

Factor		PD + IORT [n (%)]	PD (No IORT) [n (%)]	*p* value
Stage	I	7 (19)	16 (35)	0.16
	IIA	6 (16)	12 (26)	
	≥IIB	24 (65)	18 (39)	
Margin Status	RO	21 (57)	32 (70)	0.26
	R1/R2	16 (43)	14 (30)	
Grade (n=81)	Well	7 (19)	8 (18)	0.91
	Moderate	21 (58)	25 (56)	
	Poor	8 (22)	12 (27)	
Adjuvant Chemotherapy (n=79)	Yes	26 (84)	27 (63)	0.05
	No	5 (16)	16 (37)	
Adjuvant EBRT (n=75)	Yes	23 (74)	29 (66)	0.44
	No	8 (26)	15 (34)	

of IORT with LRR, with SR, and with any recurrence were conducted using logistic regression models (Table 4). After adjusting for propensity score quartile and for adjuvant therapies, IORT did not influence recurrence rates after PD for pancreatic cancer. A non-significant trend towards higher rates of any recurrence was noted for propensity scores in the third (OR 9.66, $p = 0.14$) or fourth quartile (OR 9.64, $p = 0.15$).

Discussion

Local control was not significantly different between the two groups, IORT and non-IORT, evaluated in the current series. Although the current study is limited by its retrospective design and institution bias towards treating more advanced tumors with IORT, an attempt was made to account for nonrandom allocation of patients into the IORT and non-IORT groups by using propensity score values in adjusted statistical analyses of the association of IORT with survival and recurrence. Adjuvant chemotherapy was administered to more patients in the IORT group. Although information concerning decision-making was not available, the increased rate of chemotherapy may be related to the presence of more advanced tumors in the IORT group. Despite the trends toward more advanced-stage tumors and positive resection margins in the IORT group, similar local control rates were observed.

Table 2. Location of first recurrence. Thirty patients in the IORT group and 36 patients in the non-IORT group were included in the recurrence analysis, based on availability of data to determine site of recurrence.

Site of First Recurrence	PD + IORT [n (%)]	PD (No-IORT) [n (%)]
Locoregional	7 (23)	14 (39)
Tumor Bed	6 (20)	8 (22)
Lymph Node	4 (13)	10 (28)
Locoregional-Only	2 (7)	7 (19)
Systemic	17 (57)	18 (50)
Liver	11 (37)	11 (31)
Lung/Pleura	4 (13)	7 (19)
Systemic-Only	14 (47)	11 (31)

The disparities in stage and margin status in the current study may have obscured any potential local control benefit of IORT, as these factors have been reported to negatively influence survival for patients with resected pancreatic cancer.[24, 25] Prior retrospective, single-institution reports suggest that IORT improves local control after PD by approximately 30%.[19, 21] In this study, LRR was 50% less in the IORT group. In the prospective, randomized trial conducted at the NCI, local control improved from 0% to 33% with the addition of IORT.[20] In a recent series

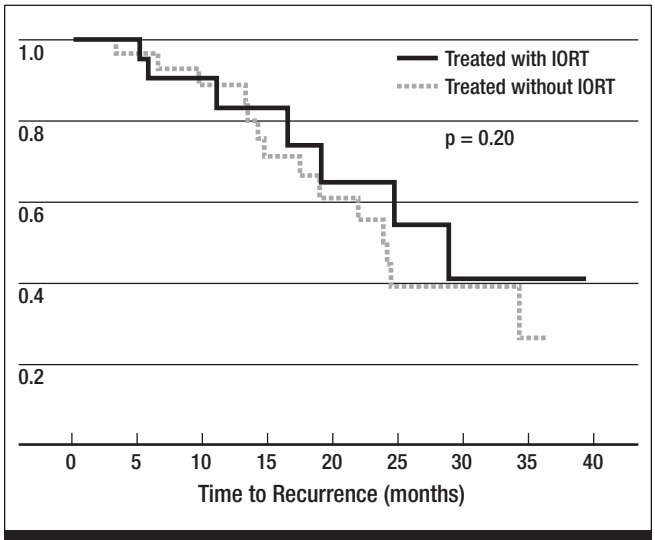

Figure 1. Kaplan-Meier plot of locoregional failure for patients treated with (*solid line*) and without (*dashed line*) IORT ($p = 0.20$).

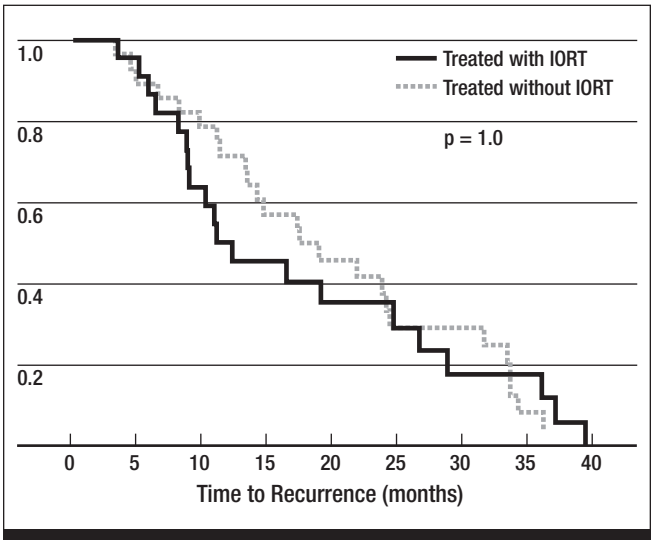

Figure 2. Kaplan-Meier plot of recurrence (any site) for patients treated with (*solid line*) and without (*dashed line*) IORT ($p = 1.0$).

Table 2. Location of first recurrence. Thirty patients in the IORT group and 36 patients in the non-IORT group were included in the recurrence analysis, based on availability of data to determine site of recurrence.

Site of First Recurrence		PD + IORT [n (%)]	PD (No-IORT) [n (%)]
Locoregional		7 (23)	14 (39)
	Tumor Bed	6 (20)	8 (22)
	Lymph Node	4 (13)	10 (28)
	Locoregional-Only	2 (7)	7 (19)
Systemic		17 (57)	18 (50)
	Liver	11 (37)	11 (31)
	Lung/Pleura	4 (13)	7 (19)
	Systemic-Only	14 (47)	11 (31)

from the City of Hope National Medical Center, isolated local recurrences were reduced from 33% to 5% with the addition of IORT, which is comparable to the rate of isolated LRR in the current report (7%).[24] Reni *et al*. reported a similar alteration of recurrence patterns, with 15% local-only recurrences with IORT versus 33% without IORT.[26] The cumulative evidence, including one prospective randomized trial and a few prospective studies, supports a local control benefit for IORT in resectable pancreatic cancer. An improvement in local control has not been shown to translate into a clinical benefit in survival outcomes, including in this study. Although a propensity score analysis was performed in the current study to evaluate the influence of IORT on recurrence rates after PD, the limited size of the patient population may have restricted our ability to detect a significant positive effect.

The survival rates were not different between the IORT and non-IORT groups in the current series, which is consistent with the results of the prospective NCI study.[20] Given the propensity of pancreatic cancer towards distant metastatic recurrence, it is not surprising that a measurable increase in local control did not produce a corresponding improvement of survival.[27] Although some authors report a survival benefit from IORT for resectable pancreatic tumors at their institutions, the literature does not consistently support this claim, and detection of a potential small survival benefit would require a large trial.[19, 22, 24, 26, 28, 29] Regardless of the absence of improved survival, the problem of locoregional control does leave open a place for radiation therapy after PD, and IORT is an effective technique to boost radiation dose around the resection bed while displacing sensitive adjacent organs.[8, 10, 17, 30] A recent analysis of the Surveillance, Epidemiology, and End Results database revealed a survival benefit to the addition of adjuvant radiotherapy after PD, and radiation therapy remains an important component of adjuvant strategies in the United States.[25] Results recently published from the Radiation Therapy Oncology Group (RTOG) trial 9704, the first cooperative group study to require prospective quality assurance of radiotherapy, suggest a benefit to the addition of gemcitabine to adjuvant CRT after PD. The rates of first relapse in local and regional sites in the experimental arm of RTOG 9704 were 23% and 7%, respectively.[31]

Table 3. Cox proportional survival hazard model for the association of IORT, propensity score, and other factors with survival time in months.

	Estimate	Standard Error	Chi-Square	Hazard Ratio	*p*
IORT	-0.34	0.35	0.94	0.71	0.33
Adjuvant Chemo-therapy	0.51	0.73	0.48	1.66	0.49
Adjuvant Radiotherapy	-1.05	0.68	2.39	0.35	0.12
Propensity Score (vs. 1st Quartile)					
2nd Quartile	-0.68	0.45	2.35	0.50	0.13
3rd Quartile	0.55	0.49	1.26	1.73	0.26
4th Quartile	0.58	0.47	1.56	1.79	0.21

Table 4. Logistic regression models of the association of IORT, propensity score, and other factors, with the outcomes of any recurrence, locoregional occurrence, and systemic recurrence.

	Odds Ratio	95% CI	*p*
Any Recurrence			
IORT	0.77	(0.19, 5.20)	0.72
Adjuvant Chemotherapy	1.69	(0.15, 19.29)	0.67
Adjuvant Radiotherapy	1.11	(0.11, 11.68)	0.93
Propensity Score (vs. 1st Quartile)			
2nd Quartile	1.22	(0.33, 4.52)	0.76
3rd Quartile	9.66	(0.47, 197.40)	0.14
4th Quartile	9.64	(0.46, 203.31)	0.15
Locoregional Recurrence			
IORT	0.41	(0.10, 10.30)	0.23
Adjuvant Chemotherapy	0.49	(0.02, 11.37)	0.65
Adjuvant Radiotherapy	1.74	(0.86, 35.51)	0.72
Propensity Score (vs. 1st Quartile)			
2nd Quartile	0.39	(0.02, 7.47)	0.53
3rd Quartile	5.13	(0.73, 36.03)	0.10
4th Quartile	3.32	(0.46, 23.93)	0.23
Systemic Recurrence			
IORT	0.99	(0.28, 3.52)	0.99
Adjuvant Chemotherapy	0.40	(0.03, 6.42)	0.52
Adjuvant Radiotherapy	1.30	(0.10, 16.96)	0.84
Propensity Score (vs. 1st Quartile)			
2nd Quartile	1.11	(0.23, 5.40)	0. 90
3rd Quartile	0.91	(0.16, 5.13)	0.91
4th Quartile	0.59	(0.10, 3.50)	0.56

Importantly, the addition of IORT after PD did not increase perioperative complication rates significantly in the current series, which is consistent with the earlier experience from our institution.[22] Although late complications have been reported after IORT for pancreatic cancer, our results and other reports suggest that IORT may be delivered safely in combination with surgical resection.[24, 26, 28, 32, 33-37] Selection of

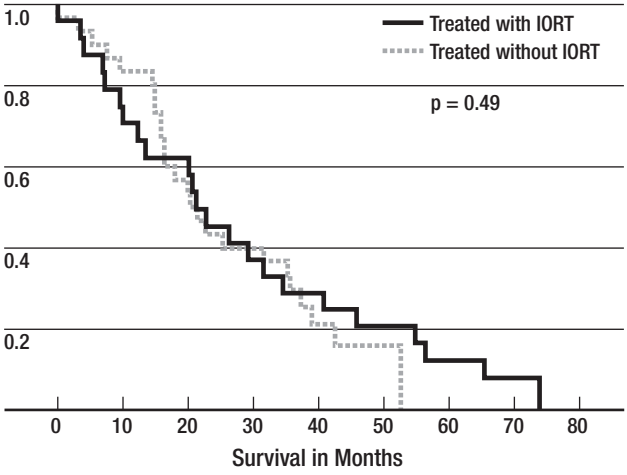

Figure 3. Cox proportional hazards model for overall survival of patients treated with (*solid line*) and without (*dashed line*) IORT after PD ($p = 0.49$).

radiation doses for IORT was influenced by seminal, preclinical canine experiments performed at the National Cancer Institute that provided an understanding of normal tissue tolerances, including surgically-manipulated tissues, for IORT.[38,39] These studies created a foundation for the rational delivery of IORT in humans, so it should not be surprising that clinical studies have shown these RT doses to be safe and feasible.

Based on recent practice changes at our institution, IORT will be offered infrequently for patients with localized pancreatic tumors, in favor of alternate adjuvant strategies after surgical resection. Novel adjuvant therapy combinations tested in recent institutional and cooperative group trials have focused on systemic treatments aimed at reducing metastatic recurrences after PD, as distant dissemination is a dominant cause of mortality for patients with pancreatic cancer.[27, 40] However, adjuvant external beam radiation therapy remains an important component of management, based on recognition of the parallel importance of preventing local recurrence.[2, 25] Although the current study does not support its continued use, it is reasonable that IORT is considered as a potential component of adjuvant RT strategies. Should adjuvant systemic therapies for resected pancreatic cancer improve in the future, LRR may become a more significant concern. IORT may become a more important tool for maximizing loco-regional control in that situation.

In summary, the current study demonstrates that IORT is a safe addition to PD and standard adjuvant therapies, with the intention of improving local control after PD for patients with resectable pancreatic cancer. Although local control was not significantly improved with the addition of IORT in the current study, the significantly higher number of more advanced stage tumors and a trend towards more positive surgical margins in the IORT patients may have influenced the results of our comparative analyses. We cannot currently recommend routine use of IORT in the adjuvant setting for patients with resected pancreatic cancer. Future clinical trials with novel therapeutic agents may include IORT in combination with resection, adjuvant external beam radiotherapy, and systemic agents in order to improve outcomes for patients with pancreatic cancer.

References

1. Sohn TA, Yeo CJ, Cameron JL, *et al.* Resected adenocarcinoma of the pancreas–616 patients: Results, outcomes, and prognostic indicators. *J Gastrointest Surg* 2000;4:567-579.
2. Willett CG, Lewandrowski K, Warshaw AL, *et al.* Resection margins in carcinoma of the head of the pancreas. *Ann Surg* 1992;217:144-148.
3. Kalser MH, Ellenberg SS. Pancreatic cancer: adjuvant combined radiation and chemotherapy following curative resection. *Arch Surg* 1985;120:899-903.
4. Gastrointestinal Tumor Study Group. Further evidence of effective adjuvant combined radiation and chemotherapy following curative resection for pancreatic cancer. *Cancer* 1987;59:2006-2010.
5. Neoptolemos JP, Stocken DD, Friess H, *et al.* A randomized trial of chemoradiotherapy and chemotherapy after resection of pancreatic cancer. *N Engl J Med* 2004;350:1200-1210.
6. Stocken DD, Buchler MW, Dervenis C, *et al.* Meta-analysis of randomised adjuvant therapy trials for pancreatic cancer. *Br J Cancer* 2005;92:1372-1381.
7. Klinkenbijl JH, Jeekel H, Sahmoud T, *et al.* Adjuvant radiotherapy and 5-fluoruracil after curative resection of cancer of the pancreas and periampullary region: Phase III trial of the EORTC Gastrointestinal Tract Cancer Cooperative Group. *Ann Surg* 1999;230:776-784.
8. Kennedy EP, Yeo CJ. The case for routine use of adjuvant therapy in pancreatic cancer. *J Surg Oncol* 2007;95:597-603.
9. Zuckerman DS, Ryan DP. Adjuvant therapy for pancreatic cancer: A review. *Cancer* 2008;2007 Nov 29 [Epub ahead of print].
10. Willett CG, Czito BG, Tyler DS. Intraoperative radiation therapy. *J Clin Oncol* 2007;25:971-977.
11. Willett CG, Del Castillo CF, Shih HA, *et al.* Long-term results of intraoperative electron beam irradiation (IOERT) for patients with unresectable pancreatic cancer. *Ann Surg* 2005;241:295-299.
12. Ma H-B, Di Z-L, Wang X-J, *et al.* Effect of intraoperative radiotherapy combined with external beam radiotherapy following internal drainage for advanced pancreatic carcinoma. *World J Gastroenterol* 2004;10:1669-1671.
13. Mohiuddin M, Regine WF, Stevens J, *et al.* Combined intraoperative radiation and perioperative chemotherapy for unresectable cancers of the pancreas. *J Clin Oncol* 1995;13:2764-2768.
14. Shipley WU, Wood WC, Tepper JE, *et al.* Intraoperative electron beam irradiation for patients with unresectable pancreatic carcinoma. *Ann Surg* 1984;200:289-294.
15. Tepper JE, Noyes D, Krall JM, *et al.* Intraoperative radiation therapy of pancreatic carcinoma: a report of RTOG-8505. *Int J Radiat Oncol Biol Phys* 1991;21:1145-1149.
16. Tuckson WB, Goldson AL, Ashayeri E, *et al.* Intraoperative radiotherapy for patients with carcinoma of the pancreas: The Howard University hospital experience, 1978-1986 *Ann Surg* 1988;207:648-653.
17. Valentini V, Balducci M, Tortoreto F, *et al.* Intraoperative radiotherapy: current thinking. *EJSO* 2002;28:180-185.
18. Willett CG, Warshaw AL. Intraoperatic electron beam irradiation in pancreatic cancer. *Frontiers in Bioscience* 1998;3:e207-213.
19. Zerbi A, Fossati V, Parolini D, *et al.* Intraoperative radiation therapy adjuvant to resection in the treatment of pancreatic cancer. *Cancer* 1994;73:2930-2935.
20. Sindelar WF, Kinsella TJ. Studies of intraoperative radiotherapy in carcinoma of the pancreas. *Ann Oncol* 1999;10:S226-S230.
21. Alfieri S, Morganti AG, Di Giorgio A, *et al.* Improved survival and local control after intra-operative radiation therapy and postoperative radiotherapy: A multivariate analysis of 46 patients undergoing surgery for pancreatic head cancer. *Arch Surg* 2001;136:343-347.
22. Farrell TJ, Barbot DJ, Rosato FE. Pancreatic resection combined with intraoperative radiation therapy for pancreatic cancer. *Ann Surg* 1997;226:66-69.
23. D'Agostino RB, Jr. Propensity score methods for bias reduction in the comparison of a treatment to a non-randomized control group. *Stat Med* 1998;17:2265-2281.
24. Schwarz RE, Smith DD, Keny H, *et al.* Impact of intraoperative radiation on postoperative and disease-specific outcome after pancreatoduodenectomy for adenocarcinoma: A propensity score analysis. *Am J Clin Oncol* 2003;26:16-21.
25. Hazard L, Tward JD, Szabo A, *et al.* Radiation therapy is associated with improved survival in patients with pancreatic adenocarcinoma: Results of a study from the Surveillance, Epidemiology, and End Results (SEER) Registry data. *Cancer* 2007;110:2191-2201.
26. Reni M, Panucci MG, Ferreri AJM, *et al.* Effect on local control and survival of electron beam intraoperative irradiation for resectable pancreatic adenocarcinoma. *Int J Radiat Oncol Biol Phys* 2001;50:651-658.
27. Hishinuma S, Ogata Y, Tomikawa M, *et al.* Patterns of recurrence after curative resection of pancreatic cancer, based on autopsy findings. *J Gastrointest Surg* 2006;10:511-518.
28. Kokubo M, Nishimura Y, Shibamoto Y, *et al.* Analysis of the clinical benefit of intraoperative radiotherapy in patients undergoing macroscopically curative resection for pancreatic cancer. *Int J Radiat Oncol Biol Phys* 2000;48:1081-1087.
29. Nishimura Y, Hosotani R, Shibamoto Y, *et al.* External and intraoperative radiotherapy for resectable and unresectable pancreatic cancer: Analysis of survival rates and complications. *Int J Radiat Oncol Biol Phys* 1997;39:39-49.
30. Newman EA, Simeone DM, Mulholland MW. Adjuvant treatment strategies for pancreatic cancer. *J Gastrointest Surg* 2006;10:916-926.

31. Regine WF, Winter K, Abrams RA, *et al.* Fluorouracil vs gemcitabine chemotherapy before and after fluorouracil-based chemoradiatino following resection of pancreatic adenocarcinoma: A randomized controlled trial. *JAMA* 2008;299:1019-1026.
32. Shimizu Y, Yasui K, Fuwa N, *et al.* Late complication in patients undergoing pancreatic resection with intraoperative radiation therapy: Gastrointestinal bleeding with occlusion of the portal system. *J Gastroenterol Hepatol* 2005;20:1235-1240.
33. Spitz FR, Abbruzzese JL, Lee JE, *et al.* Preoperative and postoperative chemoradiation strategies in patients treated with pancreaticoduodenectomy for adenocarcinoma of the pancreas. *J Clin Oncol* 1997;15:928-937.
34. Coquard R, Ayzac L, Gilly F-N, *et al.* Intraoperative radiotherapy in resected pancreatic cancer: feasibility and results. *Radiother Oncol* 1997;44:271-275.
35. Dobelbower RR, Merrick HW, Khuder S, *et al.* Adjuvant radiation therapy for pancreatic cancer: A 15-year experience. *Int J Radiat Oncol Biol Phys* 1997;39:31-37.
36. Evans DB, Termuhlen PM, Byrd DR, *et al.* Intraoperative radiation therapy following pancreaticoduodenectomy. *Ann Surg* 1993;218:54-60.
37. O'Connor JK, Sause WT, Hazard LJ, *et al.* Survival after attempted surgical resection and intraoperative radiation therapy for pancreatic and periampullary adenocarcinoma. *Int J Radiat Oncol Biol Phys* 2005;63:1060-1066.
38. Kinsella TJ, Sindelar WF. Intraoperative radiotherapy for pancreatic carcinoma. Experimental and clinical studies. *Cancer* 1996;78:598-604.
39. Sindelar WF, Kinsella TJ, Tepper JE, *et al.* Experimental and clinical studies with intraoperative radiotherapy. *Surg Gynecol Obstet* 1983;157:205-219.
40. Regine WF, Abrams RA. Adjuvant therapy for pancreatic cancer: current status, future directions.

Flexible Needle-Tissue Interaction Modeling With Depth-Varying Mean Parameter: Preliminary Study

Kai Guo Yan,[1] Tarun Podder, Member, IEEE,[2] Yan Yu,[2] Tien-I. Liu,[3] Christopher W. S. Cheng,[4] and Wan Sing Ng, Member, IEEE[5]

[1]Nanyang Technological University, Singapore; [2]Thomas Jefferson University, Philadelphia, PA, USA; [3]California State University, Sacramento, CA, USA; [4]Singapore General Hospital, Singapore; [5]Nanyang Technological University, Singapore

Abstract

Flexible needle steering has aroused a lot of research interest in recent years. It has the potential to correct targeting errors, which may be caused by needle bending, tissue deformation, or error in insertion angle. In addition, control and planning based on a steering model can guide the needle to some areas that are currently not amenable to needles because of obstacles, such as bone or sensitive tissues. Thus, there is a clear motivation for needle steering. In this paper, a spring–beam–damper model is proposed to describe the dynamics during the needle–tissue contact procedure. Considering tissue inhomogeneity, depth-varying mean parameters are proposed to calculate the spring and damper effects. Local polynomial approximations in finite depth segments are adopted to estimate the unknown depth-varying mean parameters. Based on this approach, an online parameter estimator has been designed using the modified least-square method with a forgetting factor. Some preliminary experiments have been carried out to verify the steering model with the online parameter estimator. The details are given in this paper. Finally, conclusions and future studies are given at the end.

Index Terms: Depth-varying mean parameter, needle steering modeling, percutaneous surgery, spring–beam–damper model.

I. Background

Medical procedures, such as brachytherapy, biopsies, and treatment injections, require inserting a needle to a specific target location inside the human body to implant a radioactive seed, extract a tissue sample, or inject a drug. Precise needle placement is very important. Poor placement may cause tissue damage, misdiagnosis, poor dosimetry, and tumor seeding. Unfortunately, precise needle placement is hard to achieve in real practice. Errors caused by the target movement and needle deflection have been observed for a long time.[1-4] Yet to date, there are few effective physically based needle steering systems existing for correcting the targeting error automatically when it is observed. It is interesting to note that during clinic practice, some surgeons make use of a combination of lateral, twisting, and inserting motions of the needle under visual feedback from imaging systems, such as ultrasound, to correct the targeting errors. Surgeons accomplish this from experience, making it difficult to teach and limiting the accuracy to that of human hand/eye coordination.

Flexible needle steering was first addressed by DiMaio *et al.*[5] using a finite-element model. His model was later extended by other researchers to 3-D models.[6,7] In the Medical Image Computing and Computer-Assisted Intervention Conference 2005, Daniel Glozman and Moshe Shoham[8] presented a simplified virtual spring model for the needle insertion procedure. Modeling of a flexible needle was based on the assumption of quasistatic motion and a third-order polynomial was used to calculate the displacement of each element. Compromise had to be made between the computational efficiency and the model accuracy.

Needle steering making use of the needle bending has also been explored in the past few years. Some researchers have generated needle bending using different strategies, such as incorporating a prebent stylus inside a straight canula,[9] or a telescoping double canula, where the internal canula is prebent.[10] Other researchers showed that needles with bevel tips bend more than symmetric-tip needles.[11] Making use of this effect, thin highly flexible bevel-tip needles using Nitinol were developed, and a nonholonomic model was built accordingly for steering flexible bevel-tip needles in rigid tissues.[12] The nonholonomic model, a generalization of a 3-D bicycle model, was experimentally validated using a very stiff tissue phantom. Recent advances in nonholonomic path planning include stochastic model-based motion planning to compensate for noise bias,[13] probabilistic models of dead-reckoning error in nonholonomic robots,[14] a diffusion-based motion planning to search for a feasible path in full 3-D space, and motion planning under Markov motion uncertainty using dynamic programming to search for a feasible route while avoiding obstacles.[15]

In this paper, a needle steering model is proposed for flexible needle steering purpose. A spring–beam–damper model is adopted to model the dynamics between the lateral needlebased force and the corresponding lateral needle tip movement with consideration of the needle flexibility and tissue deformation. Considering the tissue inhomogeneity, depth-varying mean parameters are proposed to calculate the spring and damper effects. Local polynomial approximations in finite-depth segments are adopted to estimate the unknown depth-varying mean parameters. Unlike the models proposed in[5] and,[8] this model takes into consideration not only the viscoelastic tissue reactions but also the tissue inhomogeneity. In the literature, the spring–damper model has been adopted by many research groups in studying tissue deformation.[16–18] But how the coupled interaction of the instrument and soft tissue is and how to control the instrument while in collision with such an environment have received little attention. Some researchers studied the collision of the flexible link with the environment in the application of grinding or surface turning operation.[19,20] They modeled the environment as a simple spring–damper system, which was assumed to be stationary and was arbitrarily placed along the trajectory such that the beam would only make contact with it at the tip. In

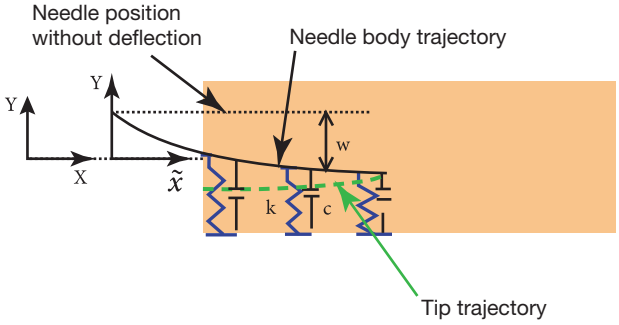

Figure 1. Mechanism of the needle insertion procedure.

the application of needle steering, the flexible instrument interacts with the environment with changing force along the needle body from time to time. The situation is much more complicated compared with the point contact.

Based on the proposed model, an online parameter estimator has been designed using the modified least-square method with a forgetting factor. Preliminary experiments have been carried out to verify the steering model with the online parameter estimator. Results have shown its effectiveness. Finally, conclusions and future studies are given at the end.

II. Needle Lateral Steering Force Modeling And Analysis

A. Needle Lateral Steering Force Modeling

A spring–beam–damper system, as shown in Fig. 1, is considered in this study to model the system dynamics between the lateral steering forces acting at the needle base and the corresponding needle tip lateral movement during insertion in the soft tissue. The flexible needle is assumed to follow the Bernoulli–Euler beam model and is required to be clamped tightly at the base. The initial lengths of springs are decided by the needle tip trajectory, as shown in the figure. At the beginning, the needle is placed next to the tissue. With time progressing on, the needle inserts into the tissue. Then, the springs and dampers come into contact with the needles and exert forces on it accordingly. The forces of the springs at time instant *t* are determined by the needle body shape at that time and the needle tip trajectory; while the forces of the dampers are determined by the velocities of the contact points. During this procedure, not only the tissue deformation and the needle flexibility, but also their interaction effects, should be taken into consideration.

To derive the equations of needle insertion, the following assumptions are made.

1) For simplicity, the needle is considered to move only in the XY plane. X is the insertion direction and Y is the steering direction.
2) There is no longitudinal compression of the beam and only lateral deflection is possible. Furthermore, the lateral deflection of the beam is small compared with the length of the beam.
3) The rotational effect of the beam with respect to the local coordinate system is neglected.

Under the aforesaid assumptions, the system dynamic equation can be derived using Hamilton's principle as follows:

$$\int_{t_1}^{t_2} (\delta T - \delta V + \delta W_{\text{nc}})\, dt = 0 \tag{1}$$

where T is the kinetic energy, V is the potential energy, and W_{nc} is the work done by nonconservative forces.

A local coordinate system is introduced by the Galilean transformation to replace the fixed coordinates (x) with a moving coordinate system ($\tilde{x}$), which is attached at the needle base and moves with it. v_x is the needle insertion velocity, which is assumed to be constant for modeling simplicity.

$$\tilde{x} = x - v_x t \quad \text{and} \quad \tilde{y} = y. \tag{2}$$

The system kinetic energy T includes the kinetic energy of the fixture and the needle, as shown in the first and second terms of the following equation (3), while the potential energy V includes the potential energy of the needle caused by needle bending (the first term) and the potential energy of the springs resulting from the forces between the needle and the tissue (the second term), as given in (4). The integration of the difference between the needle body positions and the needle tip trajectory gives the summation of the elongated or compressed spring length (decided by the sign of the difference) at the contact points. Because only the needle portion inside the tissue has springs exerting force on it (5), the Heaviside unit step function is used to exclude the portion outside the tissue. $h(x) = L - v_x t$ is the position of the insertion point in the moving coordinates system at time instant *t*. Thus, the potential energy of the springs can be calculated using the second term of (4)

$$T = \frac{1}{2}M\dot{y}^2 + \int_0^L \frac{1}{2}\rho(\dot{y}(t) + \dot{\omega}(\tilde{x}, t))^2 d\tilde{x} = T(\dot{y}, \dot{\omega}) \tag{3}$$

$$\begin{aligned} V &= \int_0^L \frac{1}{2}EI\omega''^2\, d\tilde{x} + \int_0^L H(\tilde{x} - L + v_x t) \\ &\quad \times \frac{1}{2}k\left[y(t) + \omega(\tilde{x}, t) - y\left(t + \frac{\tilde{x} - L}{v_x}\right)\right. \\ &\quad \left. - \omega\left(L, \frac{\tilde{x} - L}{v_x} + t\right)\right]^2 d\tilde{x} \\ &\xrightarrow{h(t) = L - v_x t} \int_0^L \frac{1}{2}EI\omega''^2\, d\tilde{x} + \int_0^L H(\tilde{x} - h(t)) \\ &\quad \times \frac{1}{2}k\left[y(t) + \omega(\tilde{x}, t) - y\left(\frac{\tilde{x} - h(t)}{v_x}\right)\right. \\ &\quad \left. - \omega\left(L, \frac{\tilde{x} - h(t)}{v_x}\right)\right]^2 d\tilde{x} \end{aligned} \tag{4}$$

$$H(x) = \begin{cases} 1, & x \geq 0 \\ 0, & x < 0. \end{cases} \tag{5}$$

Here, M is the mass of the fixture that links the needle with the 3-D motion platform, L is the length of the elastic beam, ρ is the mass per unit length of the elastic beam, E is the Young's modulus of the needle, I is the second moment of inertia about the z-axis, k is the stiffness coefficient of the spring per unit length, c is the damper coefficient per unit length, y is the needle base position in y-axis, $\dot{y}(t)$ is the corresponding velocity at time instant t, ω is the deflection of the beam along the needle body at time instance t, and $\dot{\omega}$ and ω'' are the first and second derivatives of the beam deflection with respect to time and space, respectively.

The virtual work done by all the nonconservative forces (steering force F_y and damping forces), is given by

$$\delta W_{\mathrm{nc}} = F_y \delta y - \int_0^L H(\tilde{x} - L + v_x t) c(\dot{y} + \dot{\omega}) \delta(y + \omega)\, d\tilde{x}. \tag{6}$$

The equation of motion and the boundary conditions of the system are obtained by substituting the aforesaid equations (3), (4), and (6) into (1), integrating the resulting equation by parts, and considering that the time $t1$ and $t2$ are arbitrary and that δy, $\delta\omega$ are arbitrary and independent. Thus, the equations of motion for the spring–damper system are obtained as follows:

$$\begin{aligned} F(y,t) = M\ddot{y} &+ \int_0^L \rho(\ddot{y} + \ddot{\omega})\, d\tilde{x} \\ &+ \int_0^L H(\tilde{x} - L + v_x t)[k(y + \omega(\tilde{x}, t) \\ &- y(t_1) - \omega(L, t_1)) + c(\dot{y} + \dot{\omega}(\tilde{x}, t))]\, d\tilde{x} \end{aligned} \tag{7}$$

$$\begin{aligned} EI\omega^{(4)} &+ \rho(\ddot{y} + \ddot{\omega}) + H(\tilde{x} - L + v_x t)[k(y + \omega(\tilde{x}, t) - y(t_1) \\ &- \omega(L, t_1)) + c(\dot{y} + \dot{\omega}(\tilde{x}, t))] = 0 \end{aligned} \tag{8}$$

where $t_1 = t + \frac{\tilde{x} - L}{v_x}$.

Boundary conditions:

$$\begin{aligned} &\text{(i) } \omega(x,0) = \omega(0,t) = 0, \ \text{(ii) } \omega'(0,t) = 0 \\ &\text{(iii) } \omega''(L,t) = \omega'''(L,t) = 0. \end{aligned} \tag{9}$$

To solve the partial differential equations shown in (7) and (8), unconstrained modal analysis is adopted in this approach.[21] The deflection of the elastic beam and the displacement of the fixture are expressed, respectively, in terms of n mode shapes using the obtained $\varphi(\tilde{x})$, β_i, $q_i(t)$ as follows:

$$\omega(\tilde{x}, t) = \sum_{i=1}^{n} \phi_i(\tilde{x}) q_i(t) = \sum_{i=1}^{n} [\varphi_i(\tilde{x}) - \beta_i] q_i(t) \tag{10}$$

and accordingly, the position of fixture is given as

$$y(t) = \alpha(t) + \sum_{i=1}^{n} \beta_i q_i(t) \tag{11}$$

where $\alpha(t)$ describes the motion of the center of mass of the total system without perturbation, $\phi(\tilde{x})$ is the shape function that is the space solution of the deflection, $q(t)$ is the time-varying amplitude of motion that is the time solution of the deflection, and β is defined to satisfy

$$\beta = -\frac{\rho}{M_t} \int_0^L \phi(\tilde{x})\, d\tilde{x}. \tag{12}$$

After some algebraic manipulation (refer to [22] for more details), the model is finally obtained as follows:

$$\begin{aligned} &\dot{\alpha}(t) \int_{L - v_x t}^{L} c\varphi_i(\tilde{x})\, d\tilde{x} + \alpha(t) \int_{L - v_x t}^{L} k\varphi_i(\tilde{x})\, d\tilde{x} \\ &+ \sum_j^n \dot{q}_j(t) \int_{L - v_x t}^{L} c\varphi_i(\tilde{x})\varphi_j(\tilde{x})\, d\tilde{x} \\ &+ \ddot{q}_i(t) + \sum_j^n q_j(t) \int_{L - v_x t}^{L} k\varphi_i(\tilde{x})\varphi_j(\tilde{x})\, d\tilde{x} + \xi_i^2 q_i(t) \\ &= F_y \beta_i + f_{1i} \end{aligned} \tag{13}$$

$$\begin{aligned} &M_t \ddot{\alpha}(t) + c v_x \dot{\alpha}(t) t + \sum_j^n \dot{q}_j(t) \int_{L - v_x t}^{L} c\varphi_j(\tilde{x})\, d\tilde{x} \\ &+ k v_x \alpha(t) t + \sum_j^n q_j(t) \int_{L - v_x t}^{L} k\varphi_j(\tilde{x})\, d\tilde{x} = F_y + f_2 \end{aligned} \tag{14}$$

with

$$\begin{aligned} f_{1i} &= \int_0^t k\alpha(t_1)\varphi_i(v_x t_1 + L - v_x t) v_x\, dt_1 \\ &\quad + A \int_0^t k \sum_j^n \varphi_j(L) q_j(t_1) \varphi_i(v_x t_1 + L - v_x t) v_x\, dt_1 \\ &= \int_0^t kY(t_1)\varphi_i(v_x t_1 + L - v_x t) v_x\, dt_1 \\ f_2 &= \int_0^t k\alpha(t_1) v_x\, dt_1 + \int_0^t k \sum_j^n \varphi_j(L) q_j(t_1) v_x\, dt_1 \\ &= \int_0^t kY(t_1) v_x\, dt_1. \end{aligned}$$

Here, M_t is the total mass of the fixture and needle; $Y(t_1) = \alpha(t) + \sum_{i=1}^{n} \varphi_i(L) q_i$ is the needle tip position at time instant t_1, which is time varying and derived from (10)–(12); and F_y is the lateral steering force, which acts at the needle base in the y direction.

These partial differential equations can be solved using the explicit Runge–Kutta (4, 5) formula, and the Dormand–Prince pair. A Matlab simulation program has been composed to simulate this model. With the applied needle base force F_y serving as the input of the model, α and q_i will change with time, thus causing the change of the needle tip position $Y(t_1)$ in the y-axis, which is the output of the model, as well as the tissue reaction forces.

B. Local Polynomial Approximation of Depth-Varying Mean Parameters

Considering the inhomogeneous human tissue and the multiple tissue layers that the needle will penetrate through during surgery, here we

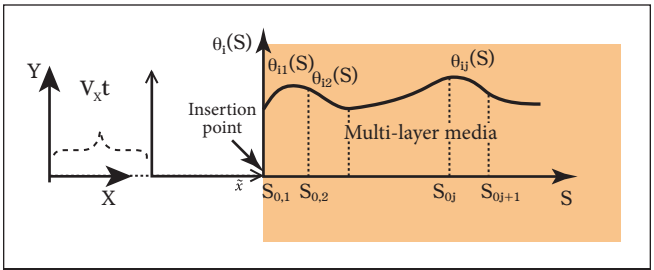

Figure 2. Local polynomial approximations of the parameter functions.

propose to use depth-varying mean parameters to calculate the spring/damper reaction forces and use local polynomials to approximate the depth-varying mean parameters.

Assumption 1: The spring and damper coefficients are different at different depths of the tissue. At each insertion step, the spring/damper effects along the needle body that is inside the tissue can be calculated using mean spring/damper coefficients $\theta(s) = [\bar{c}\ \bar{k}]^T$. These mean coefficients will vary with each step.

This assumption takes into consideration the inhomogeneous human tissue, and at the same time, releases the computation intensity by using mean values to calculate the spring/damper forces along the needle body at each insertion step. Furthermore, the adoption of the mean values guarantees that $\theta(s)$ is continuously distributed regardless of the abrupt change of the tissue properties, e.g., pathological changes of the tissue, or multilayer insertion.

Assumption 2: The depth-varying mean parameters $\theta(s)$ can be represented by a series of local polynomial approximations in finite segments.

This can be justified using Taylor series expansion. Recall that the functions $\theta(s)$ can be expanded around certain points s_0, as shown next. Here, $\theta(s)$ is approximated by the first p + 1terms. The last term represents the error due to the approximation

$$\theta(s) = \theta(s_0) + (s - s_0)\theta^{(1)}(s_0) + \cdots + \frac{(s - s_0)^p}{p!}\theta^{(p)}(s_0) + \int_{s_0}^{s} \frac{(s - \xi)^{p+1}}{(p+1)!}\theta^{(p+1)}(\xi)\, d\xi. \quad (15)$$

From the aforesaid assumptions, we can divide the whole insertion length into several segments and adopt piecewise continuous p-order differentiable functions θ_{ij}, $i = 1, 2, j = 1, 2, \ldots, n$ to represent the depth-varying mean parameter $\theta_i(s)$, $i = 1, 2$ in each segment, as illustrated in Fig. 2. Here, the index i refers to the ith parameter (spring or damper coefficient), while the index j refers to the jth segment and n is the number of segments. The S coordinate system is adopted for convenient representation of the parameters. So, the polynomial approximation of θ_{ij} is represented as

$$\begin{aligned}\theta_{ij}(s) &= a_{ij0}(s_{0,j}) + a_{ij1}(s_{0,j})(s - s_{0,j}) \\ &\quad + \cdots + a_{ijp}(s_{0,j})(s - s_{0,j})^p \\ &:= \sum_{k=0}^{p} a_{ijk}(s_{0,j})(s - s_{0,j})^k \\ &:= \varphi_{ij}^T(s, s_{0,j}) A_{ij}(s_{0,j}), s \in [s_{0,j}, s_{0,j} + l) \end{aligned} \quad (16)$$

where l is the length of the segment and p is the order of the polynomial. $s_{0,j}$ refers to the resetting depth at which the jth window of the local polynomial approximation for parameter θi begins. $s_{0,j}$ is given by the sequence $s_0 = \{s_{0j}\}$, $j = 1, \ldots, n$ and $s_{0,(j+1)} - s_{0,j} = l$. $a_{ijk}(s_{0,j}) = (1/k!)\theta_{ij}^{(k)}(s_{0,j}), k = 0, \ldots, p$, where $\theta_{ij}^{(k)}(s_{0,j})$ is the kth depth derivative evaluated at $s = s_{0,j}$. $A_{ij}(s_{0,j}) := [a_{ij0}(s_{0,j}), a_{ij1}(s_{0,j}), \ldots, a_{ijp}(s_{0,j})]^T$ is the unknown constant vector and $\varphi_{ij}^T(s, s_{0,j}) := [1, (s - s_{0,j}), \ldots (s - s_{0,j})^p]$ is a column vector. Notice that $A_{ij}(s_{0,j})$ is constant only within each segment $[s_{0,j}, s_{0,j+1})$, and in general, differs from one segment to another for the inhomogeneous tissue.

Therefore, it is possible to use (16) to approximate $\theta_{ij}(s)$ more precisely by choosing either a higher order polynomial, that is, p large, or a smaller segment l, or both. If we partition the whole insertion length into segments with the length of each segment equal to l, then the depth-varying function $\theta_i(s)$ can be approximated by a number of polynomials $\theta_{ij}(s)$ located in each segment with constant coefficients a_{ijk}, as shown in (16).

C. Online Parameter Estimator Design

The discretized needle steering model is considered here. The needle steering force model can be reorganized as

$$M\ddot{x} + c\Pi\dot{x} + (k\Pi + \Pi_1)x = u - kH \quad (17)$$

where

$$x = \begin{pmatrix} \alpha \\ q \end{pmatrix}, M = \begin{pmatrix} M_t & 0 \\ 0 & 1 \end{pmatrix}, u = \begin{pmatrix} 1 \\ \beta \end{pmatrix} F_y$$

$$\Pi_1 = \begin{pmatrix} 0 & 0 \\ 0 & \omega^2 \end{pmatrix}, \Pi = \begin{pmatrix} v_x t & \int_{L - V_x t}^{L} \varphi(\tilde{x})\, d\tilde{x} \\ \int_{L - V_x t}^{L} \varphi(\tilde{x})\, d\tilde{x} & \int_{L - V_x t}^{L} \varphi^2(\tilde{x})\, d\tilde{x} \end{pmatrix}$$

$$H = \begin{pmatrix} \int_0^t y_1(t_1) v_x\, dt_1 \\ \int_0^t \varphi_1(v_x t_1 + L - v_x t) y_1(t_1) v_x\, dt_1 \end{pmatrix}.$$

The measured output

$$Y(t) = \begin{pmatrix} y_1 \\ y_2 \end{pmatrix} = \underbrace{\begin{pmatrix} 1 & \varphi(L) \\ 1 & \varphi(0) \end{pmatrix}}_{B} x = Bx. \quad (18)$$

Here, y_1 refers to the needle tip trajectory, while y_2 is the needle base trajectory that is measured to facilitate the computation of the system state x.

After some algebraic manipulation, we can get

$$Z_k = \Phi_{k-1}^T \bar{\theta} \quad (19)$$

where $Z_k = Y_k, \Phi_{k-1}^T = [-TBM^{-1}\Pi_{k-2}B^{-1}(Y_{k-1} - Y_{k-2}) - T^2BM^{-1}(\Pi_{k-2}B^{-1}Y_{k-2} + H_{k-2})\quad 2Y_{k-1} - Y_{k-2} + T^2BM^{-1}u_{k-2} - BM^{-1}\Pi_{1k}B^1Y_{k-2}]$, and $\bar{\theta} = [\bar{c}\quad \bar{k}\quad 1]^T \in R^m$ is the unknown depth-varying mean parameter vector with an additional constant 1.

Substituting the polynomial approximations for the depth-varying mean parameters, (19) can be represented as

$$Z_k = \Phi_{k-1}^T \bar{\theta} = \underbrace{\Phi_{k-1}^T \begin{bmatrix} \varphi^T(s, s_{0,j}) & & \\ & \varphi^T(s, s_{0,j}) & \\ & & 1 \end{bmatrix}}_{\mathrm{X}_{k-1}^T} \underbrace{\begin{bmatrix} A_1 \\ A_2 \\ 1 \end{bmatrix}}_{\vartheta}$$

$$:= \mathrm{X}_{k-1}^T \vartheta s. \tag{20}$$

Here, for simplicity, we select the same-order polynomials for the two parameters.

The transformation between the s domain and $\tilde{x}$ domain is given by

$$\begin{cases} \tilde{x} = s + L - \dot{s}t \\ \dot{s} = v_x \end{cases} \tag{21}$$

under the same assumption that the needle is inserted at constant velocity.

$$t_0 := \left\{ t_{0,j} = \frac{s_{0,j}}{v_x} \right\}, \qquad j = 1, 2, \ldots. \tag{22}$$

To facilitate the computation of the dynamic equation, the dataset $s_0 = \{s_{0,j}\}, j = 1, 2, \ldots$ can be converted to the time domain using

In discretized form

$$k_{0,j} = \{t_{0,j}/T\}, \qquad j = 1, 2, \ldots, n. \tag{23}$$

Based on this approach, the modified least-square estimation with covariance resetting and forgetting factor is adopted to estimate the coefficients that take the form

$$\begin{aligned} \hat{\vartheta}_k &= \hat{\vartheta}_{k-1} + K_k(Z_k - \mathrm{X}_{k-1}^T \hat{\vartheta}_{k-1}) \\ K_k &= P_{k-1} X_{k-1} [\lambda I + \mathrm{X}_{k-1}^T P_{k-1} X_{k-1}]^{-1} \\ P_k &= [P_{k-1} - K_k \mathrm{X}_{k-1}^T P_{k-1}]/\lambda \end{aligned} \tag{24}$$

where $\hat{\vartheta}$ is the estimated parameter vector, Z is the measurement, λ is the forgetting factor, P is the covariance matrix, and K is the gain.

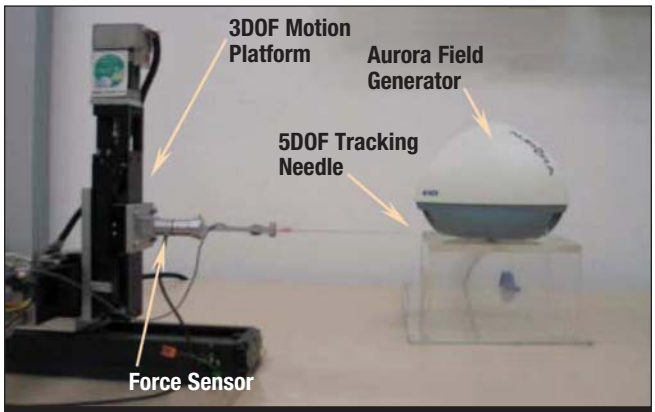

Figure 3. Experimental setup.

D. Lateral Steering Force Model Validation

1) Material and Method:

To validate the effectiveness of the proposed steering model, a physical experiment has been carried out. The experimental setup, shown in Fig. 3, is used to carry out the experiment. The 3-DOF motion platform drives the needle into the phantom/animal organ following some predesigned trajectory. A 6-DOF force/torque (F/T) sensor is mounted at the needle base to measure the needle base force. The needle adopted here is a 5-DOF MagTrax needle probe. It is a 130-mm-long needle and has a sensor located at the stylet's proximal symmetric tip. This needle tip movement in the 5-DOF, except rotation about the needle axis, can be observed in real time via an electromagnetic system called Aurora.

An "active" way of validating the proposed model by steering the needle tip to a defined position is infeasible now, since it will require a steering strategy, which is our future task. Instead, a "passive" way of validation is adopted to show that the model could accurately predict the needle tip trajectory when giving some inputs – needle-based lateral forces. The detailed validation procedure is described as follows.

The needle is first driven into the prepared phantom by the 3-DOF platform following some predetermined trajectories with various insertion speeds. The needle tip/base positions and corresponding needle base force data are collected during the procedure. These collected datasets are first passed through a designed filter to remove the measurement noises and smooth the data. After that, the filled datasets go through the online parameter estimator to estimate the depth-varying mean parameters. At the same time, the model is simulated using the online estimated parameters and the collected dataset to predict the output, the needle tip position. The output is then regulated using the collected output data instead of the simulated ones during the simulation. This regulation method can prevent the simulator from accumulating estimation errors, which will gradually lead to the divergence of the estimation. At last, the simulated outputs and the needle tip position data are compared with the measured positions during experiments.

2) Preliminary Experiments in Tissue-Like Phantoms:

Phantoms made of different gelatin/water ratios were first adopted to simulate the soft tissue, for it is easy to obtain and the properties are easy to control and replicate. The needle was driven into the phantom for 8 cm in the x-direction and 2 cm in the y-direction. The insertion speed was set to be 8, 4, and 2 mm/s, respectively. The lateral speed was chosen accordingly in order to keep the movements in x and y to start and stop simultaneously.

Fifth-order polynomials were chosen to represent the spring and damper coefficients. The initial coefficients were set to be [$3 \times 10^5 \times$ ones (6, 1); $2 \times 10^6 \times$ ones(6, 1); 1]. The initial covariance matrix was set to be [$10^{16} \times$ eye(13, 12)zeros(13, 1)]. The forgetting factor was selected to be 0.99. For comparison purpose, one segment was chosen first. Fig. 4 shows one typical example of the simulated output versus the measured output. The corresponding measurement errors and the reconstructed depth-varying mean spring/damper coefficients using the estimated polynomial parameters are shown in Figs. 5–7.

To improve the tracking accuracy, two segments were chosen next. The same initial settings were used as in the one-segment estimation. The simulation errors of one-segment estimation and two-segment estimation are compared and shown in Fig. 8. We can see that the overall accuracy has improved when using two segments.

Fig. 4

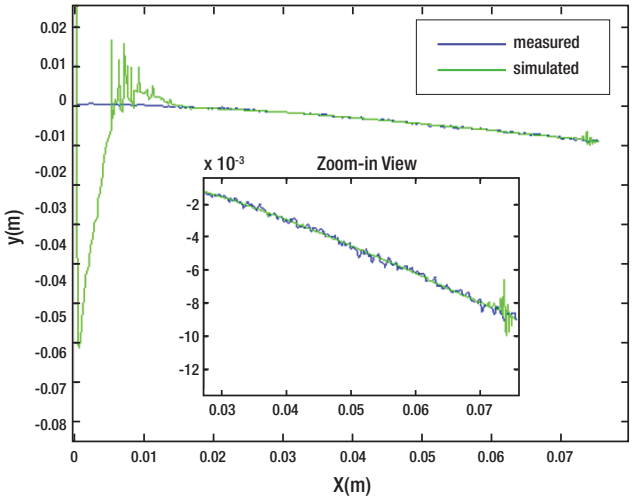

Fig. 5

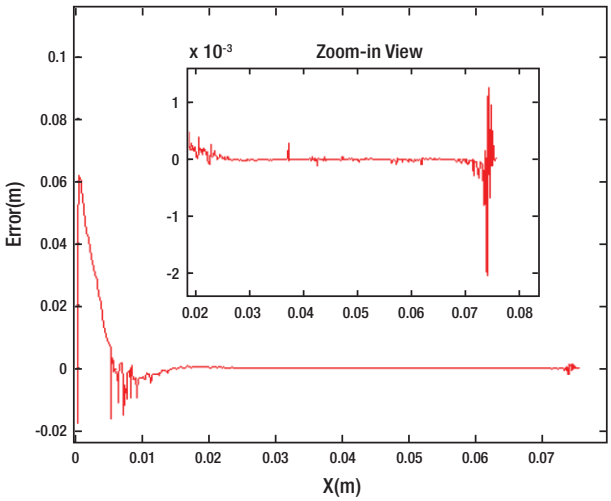

Figure 4. Simulated versus measured tip trajectories.
Figure 5. Simulation errors.
Figure 6. Estimated depth-varying spring coefficients.
Figure 7. Estimated depth-varying damper coefficients.
Figure 8. Error comparisons.

3) Discussion:

In this set of gelatin experiments, fifth-order polynomials were adopted for the spring and damper coefficients. Orders lower than fifth have shown larger estimation errors; while orders larger than fifth can give better accuracy, but no significant improvement. Dividing the whole insertion depth into more segments will improve the overall tracking accuracy, but not much improvement on the convergent rate, as can be detected in Fig. 8. The large estimation errors at the beginning were caused by poor initial estimation and the large sensor noises due to the sudden oscillation of the sensors when the needle was

Fig. 6

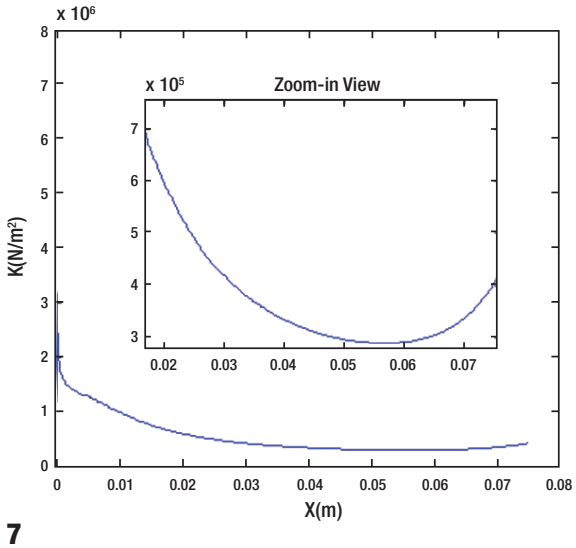

Fig. 7

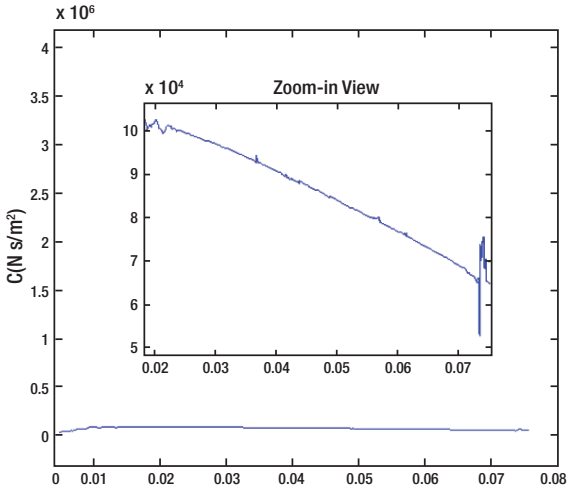

Fig. 8

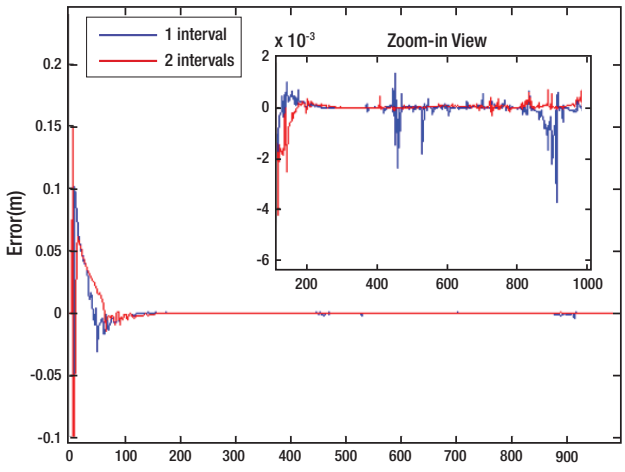

accelerated to penetrate into the phantom; the relatively large estimation errors at the end were due to the erratic sensor output when the needle was decelerated to stop. The adjustment of the initial estimation has been found to be capable of decreasing the magnitude of the initial estimation error but cannot give much improvement on the convergent rate. This will be further investigated in later experiments.

The initial covariance matrix with magnitude larger than 10^{16} showed a better convergent rate, but not much improvement could be achieved especially when the magnitude is larger than 10^{18}; less than 10^{16} would give a poor convergent rate with a decrease in overall accuracy.

The design of the online parameter estimator guarantees that the estimated coefficients will lead to minimum errors between the measured and estimated needle positions; this means that the process and measurement errors during the procedure may be incorporated into the parameter estimates, which is allowable since our goal is to achieve accurate needle position prediction, instead of precise parameter estimation. That is why even in the homogeneous gelatin phantom, the estimated spring/damper coefficients were found to be nonuniform in depth. In addition, the estimation is specific to the chosen trajectory. Thus, even in the same medium, it is highly possible that the estimated parameters will be different when choosing different trajectories.

More experiments will be carried out in the near future to further test the robustness of the steering model, as well as finding a method to improve the convergent rate.

III. Conclusion And Future Work

A needle steering model is proposed in this paper. Considering the tissue inhomogeneity, depth-varying mean parameters are adopted to calculate the tissue reaction effects. Local polynomials in finite segments are adopted to approximate the unknown depth-varying mean parameters. Based on this approach, an online parameter estimator has been designed using the modified least square method with a forgetting factor. Some preliminary experiments have been carried out to verify the steering model with the online parameter estimator. Results have shown its effectiveness. More experiments will be carried out in the near future to test the robustness of the steering model and improve the convergent rate.

In the future, we will use the proposed needle steering model with an online parameter estimator to design an adaptive needle steering system that can steer the needle tip following some prescribed trajectory. The Aurora system and force sensor system can be adopted to measure the needle tip positions and needle base forces during the procedure.

References

1. J. Pouliot, R. Taschereau, C. Cot'e, J. Roy, and D. Tremblay, "Dosimetric aspects of permanent radioactive implants for the treatment of prostate cancer," *Phys. Can.*, vol. 55, no. 2, pp. 61–68, 1999.
2. R. Taschereau, J. Roy, and J. Pouliot, "Monte Carlo simulations of prostate implants to improve dosimetry and compare planning methods," *Med. Phys.*, vol. 26, no. 9, pp. 1952–1959, 1999.
3. R. Alterovitz, J. Pouliot, R. Taschereau, I.-C. Hsu, and K. Goldberg, "Needle insertion and radioactive seed implantation in human tissues: Simulation and sensitivity analysis," in *Proc. IEEE Int. Conf. Robot. Autom.* Sep. 14–19, 2003, vol. 2, pp. 1793–1799.
4. R. Alterovitz, J. Pouliot, R. Taschereau, I.-C. J. Hsu, and K. Goldberg, "Sensorless planning for medical needle insertion procedures," in *Proc. IEEE/RSJ Int.Conf. Intell. Robots Syst.* Oct. 27–31, 2003, vol. 3, pp. 3337–3343.
5. S. P. DiMaio, "Modelling, simulation and planning of needle motion in soft tissues," Ph.D. dissertation, Univ. Br. Columbia, 2003.
6. J. Hing, A. D. Brooks, and J. P. Desai, "Reality-based estimation of needle and soft-tissue interaction for accurate haptic feedback in prostate brachytherapy simulation," presented at the *Int. Symp. Robot. Res.*, San Francisco, CA, Oct. 2005.
7. O. Goksel, "3D needle–tissue interaction simulation for prostate brachytherapy," in *Proc. 15th Annu. Can. Conf. Intell. Syst.*, 2005, pp. 827–834.
8. D. Glozman andM. Shoham, "Flexible needle steering and optimal trajectory planning for percutaneous therapies," in *Proc. Med. Imag. Comput. Comput.-Assist. Interv.*, 2004, pp. 137–144.
9. R. Ebrahimi, S. Okzawa, R. Rohling, and S. Salcudean, "Hand-held steerable needle device," in *Proc.Med. Imag. Comput. Comput.-Assist. Interv.*, 2003, vol. 2879, pp. 223–230.
10. W. Daum, "A deflectable needle assembly," Patent 5 572 593, 2003.
11. M. D. O'Leary, C. Simone, T.Washio, K. Yoshinaka, and A.M. Okamura, "Robotic needle insertion: Effects of friction and needle geometry," in *Proc. IEEE Int. Conf. Robot. Autom.* Sep. 14–19, 2003, vol. 2, pp. 1774–1780.
12. R. J. Webster III, N. J. Cowan, G. Chirikjian, and A. M. Okamura, "Nonholonomic modeling of needle steering," *Int. J. Robot. Res., vol. 25*, no. 5-6, pp. 509–525, 2006.
13. Y. Zhou and G. S. Chirikjian, "Planning for noise-induced trajectory bias in nonholonomic robots with uncertainty," in *Proc. IEEE Int. Conf. Robot. Autom.*, Apr. 26–May 1, 2004, vol. 5, pp. 4596–4601.
14. Y. Zhou and G. S. Chirikjian, "Probabilistic models of dead-reckoning error in nonholonomic mobile robots," in *Proc. IEEE Int. Conf. Robot. Autom.*, Sep. 14–19, 2003, vol. 2, pp. 1594–1599.
15. R. Alterovitz, A. Lim, K. Goldberg, G. S. Chirikjian, and A. M. Okamura, "Steering flexible needles under Markov motion uncertainty," in *Proc. IEEE/RSJ Int. Conf. Intell. Robots Syst. (IROS)*, Aug. 2005, pp. 120–125.
16. D. Terzopoulos and K. Waters, "Analysis and synthesis of facial image sequences using physical and anatomical models," *IEEE Trans. Pattern Anal. Mach. Intell.*, vol. 15, no. 6, pp. 569–579, Jun. 1993.
17. F. Boux de Casson and C. Laugier, "Modelling the dynamics of a human liver for a minimally invasive surgery simulation," Lecture Notes in Computer Science, in *Proc.Med. Imag. Comput. Comput.-Assist. Interv.*, 1999, vol. 1679, pp. 1156–1165.
18. P. F. Neumann, L. L. Sadler, and J. Gieser, "Virtual reality vitrectomy simulator," in *Proc. MICCAI*, 1998, vol. 1496, pp. 910–917.
19. M.-C. Lu and E. Kannatey-Asibu Jr., "Flank wear and process characteristic effect on system dynamics in turning," *J. Manuf. Sci. Eng.*, vol. 126, no. 1, pp. 131–140, 2004.
20. F. M. C. Ching and D. Wang, "Exact solution and infinite-dimensional stability analysis of a single flexible link in collision," *IEEE Trans. Robot. Autom.*, vol. 19, no. 6, pp. 1015–1019, Dec. 2003.
21. C. Canudas deWit, B. Siciliano, and G. Bastin, *Theory of Robot Control.* New York: Springer-Verlag, 1996.
22. K. Yan, W. S. Ng, Y. Yu, T. Podder, T.-I. Liu, C. W. S. Cheng, and K. V. Ling, "Needle steering modeling and analysis using unconstrained modal analysis," in *Proc. 1st IEEE Int. Conf. Robot. Autom. Soc. Biomed. Robot. Biomechatronics*, Italy, 2006, pp. 87–92.

Departmental Information

Thomas Jefferson University
Jefferson Medical College
Department of Radiation Oncology

Kimmel Cancer Center – Bodine
111 S. 11th Street
Philadelphia, PA 19107
Telephone: 215-955-6700
Patient Appointments: 215-955-6702
www.kimmelcancercenter.org/kcc/radonc/bodine.htm

FACULTY

Clinicians

Adam P. Dicker, MD, PhD
Interim Chair

Peter H. Ahn, MD
P. Rani Anné, MD
Tithi Biswas, MD
Jessie W. DiNome, MD
Scot A. Fisher, DO
Eric L. Gressen, MD
Arthur J. Harvey, MD
Richard (Yaacov) Lawrence, MD
Jeffrey G. Rosenstock, MD
Shari B. Rudoler, MD
Merrill J. Solan, MD
Timothy N. Showalter, MD
Maria Werner-Wasik, MD

Division of Molecular Radiobiology

Adam P. Dicker, MD, PhD
Division Director

Ronald A. Coss, PhD
Dennis B. Leeper, PhD
Qing Ren, MD, PhD
Phyllis R. Wachsberger, PhD

Division of Medical Physics

Yan Yu, PhD, MBA
Division Director

Junsheng Cao, MS
Laura Doyle, MS
Lei Fu, MS
James M. Galvin, DSc
Amy Harrison, MS
Jun Li, PhD
Haisong Liu, PhD
Harold Perera, PhD
Tarun Podder, PhD
Ying Xiao, PhD

Research: Department of Radiation Oncology

Clinical Research Studies/Grants

- Phase I Study of the Combination of Vorinostat and Radiation Therapy for the Treatment of Patients with Brain Metastases.
- A Phase I Study Evaluating the Safety, Tolerability and Pharmaco-kinetics of ABT-888 in Combination with Whole Brain Radiation Therapy in Subjects with Brain Metastases.
- A Phase II Study of Erlotinib (Tarceva) and Hypofractionated Thoracic Radiotherapy for Patients with Advanced or Inoperable Non-Small-Cell Lung Cancer.
- RTOG #0436: A Phase III Trial Evaluating the Addition of Cetuximab to Paclitaxel, Cisplatin, and Radiation for Patients with Esophageal Cancer Who are Treated Without Surgery.
- RTOG #0534: A Phase III Trial of Short Term Androgen Deprivation with Pelvic Lymph Node or Prostate Bed Only Radiotherapy (SPPORT) in Prostate Cancer Patients with a Rising PSA after Radical Prostatectomy
- RTOG #0614: A Randomized, Phase III, Double-Blind, Placebo-Controlled Trial of Memantine for Prevention of Cognitive Dysfunction in Patients Receiving Whole-brain Radiotherapy.
- RTOG #0825: Phase III Double-Blind, Placebo-Controlled Trial of Conventional Concurrent Chemo-radiation and Adjuvant Temozolomide Plus Bevacizumab Versus Conventional Concurrent Chemoradiation and Adjuvant Temozolomide in Patients with Newly Diagnosed Glioblastoma.

Basic Research Studies/Grants

- Role of PIDD (LRDD) in coordinating the p53 and NFkB pathways' response to genotoxic stress.
- Self-seeding and radiation therapy: A new strategy against metastatic prostate cancer.
- Dynamic control and tumor tracking for high duty cycle precise radiation therapy.
- Improvement of GBM control by combining the HDAC inhibitor, Vorinostat, with radiation and Temozolomide.
- ACRIN Protocol 6688: PET Pre-and post treatment assessment for locally advanced non-small cell lung carcinoma.
- RTOG Group Member Agreement.
  - Physicist Chair
  - Deputy Group Chair
  - Vice Chair Translational Research Program
  - Ultrasound-encoded functional optical imaging.
- Improvement of local control in locally advanced prostate cancer by combining the mTOR Inhibitor Temsirolimus with ionizing radiation.
- Molecular determinants of glioblastoma response to Temozolamide combined with AZD2171 and radiotherapy.
- Development and analysis of an infrastructure for review of modern clinical trials that include radiotherapy analysis.

Support Groups

Call for more details

Jefferson Journaling: A Program for Women Facing Cancer
We will provide you techniques and tools for journaling. Join us and find out how journaling may help you to reduce stress related to illness or everyday life. Please feel free to invite a supportive family member or friend. *Call **1-800-JEFF-NOW**.*

Buddy Program and Buddy-on-the-Spot
A program in which newly diagnosed cancer patients are matched (by diagnosis, treatment, age, and gender) with a trained cancer survivor for one-on-one telephone support; on-site support in Radiation Oncology or Medical Oncology Infusion. *Call **215-955-8370**.*

Reduce Stress and Live Better – A Program for Women with Cancer
This research study focuses on learning skills for living better with the stress of cancer. The program includes free 8-week cancer support programs for women, 21 years or older, and diagnosed with cancer or a recurrence within three years (including those in active treatment). *Call **215-955-2881** or visit: **www.jeffersonhospital.org/cim***

Ongoing Programs

Every Thursday

Radiation Therapy Information Session
This education and support program is for individuals receiving radiation therapy. It is recommended that people attend this session either prior to starting or in the first few weeks of treatment. Physical and psychosocial effects of radiation therapy are discussed.

Time: 10 – 11 am
Location: Kimmel Cancer Center
Bodine Building, G-312
Simon Kramer Conference Room
111 S. 11th Street, Philadelphia, PA 19107

You can find additional information on our programs and services for patients and their families at
www.JeffersonHospital.org/cancer/programs.html

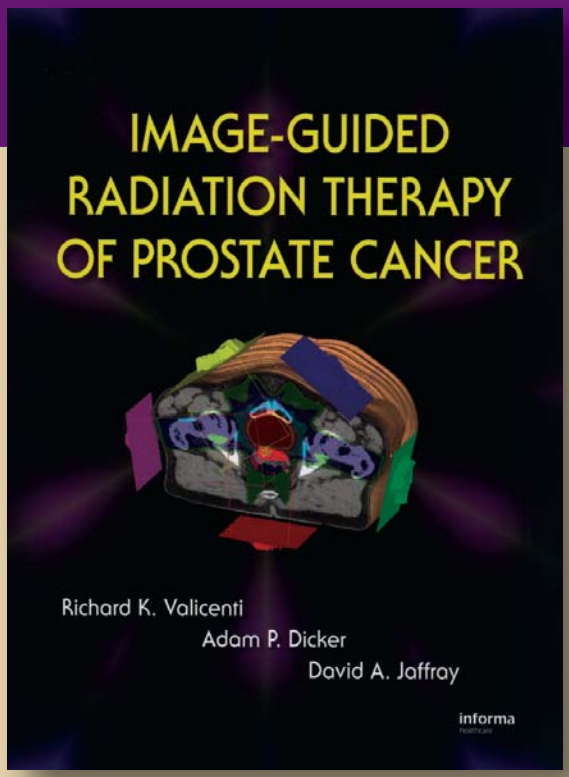

An outstanding new title from Informa Healthcare

Image-guided Radiation Therapy For Prostate Cancer: Principles And Practice

Richard K. Valicenti
Thomas Jefferson University Hospital
Philadelphia, Pennsylvania, U.S.A.

Adam P. Dicker
Thomas Jefferson University Hospital
Philadelphia, Pennsylvania, U.S.A.

David A. Jaffray
Princess Margaret Hospital, Toronto
Ontario, Canada

May 2008 / ISBN-13: 9781420060782
312 pp. / 158 Illustrations / **Price: $229.95**

Answering the need that exists for a single reference to address the practical issues of implementing image guided radiation therapy (IGRT) into prostate cancer treatment, this text provides:

- complete overview of new and exciting technologies
- practical guidance on successfully employing IGRT to improve patient outcomes
- disease stage-specific recommendations which include dosage, fractionation, target volume delineation, and tissue tolerances
- latest novel approaches to radiotherapy of prostate cancer that include intensity modulated radiation therapy (IMRT), hypofractionated radiation therapy, and proton beam radiation therapy

Contents Include:

- Overview and treatment guidelines for image-guided treatment in prostate cancer management
- Imaging modalities
- Modeling potential benefits from IGRT
- Pelvic and prostate anatomy, implications for IGRT
- Image-guided treatment planning and localization modalities
- Image-guidance: the urologist perspective
- IGRT in prostate cancer: focus on fiducials
- IGRT in prostate cancer: focus on BAT and ultrasound
- IGRT in prostate cancer: focus on adaptive therapy
- IGRT in postoperative RT for prostate cancer
- The use of image-guidance in prostate brachytherapy
- IGRT in prostate cancer: targeting pelvic lymph nodes
- Fractionation issues with IGRT for clinically localized prostate cancer
- Image-guided proton beam radiotherapy
- Future developments: On-line dosimetric verification and cone-beam RT planning and verification

Ordering Information

PHONE North America 1-800-634-7064
South America 1-859-727-5000
Int'l +44 (0) 1264 343071

FAX North America 1-800-248-4724
South America 1-859-647-4028
Int'l +44 (0) 1264 343005

E-MAIL orders@taylorandfrancis.com
INTERNET www.amazon.com or www.bn.com
MAIL Informa Healthcare
Kentucky Distribution Center
7625 Empire Drive
Florence, KY 41042 U.S.A.

JG 10-1063 MC 09-01339

Jefferson®
Kimmel Cancer Center
NCI-designated